Piotr Bernatowicz

Cross - correlations of nuclear quadrupolar interactions in the studies on molecular structure and dynamics in liquids

Cross-correlations of nuclear quadrupolar interactions in the studies on molecular structure and dynamics in liquids.

Piotr Bernatowicz

Institute of Organic Chemistry
Polish Academy of Sciences

Thesis performed under supervision of
prof. dr. hab. Lech Stefaniak and dr. hab. Sławomir Szymański

Warsaw, March 2001

I wish to express my sincere appreciation to my supervisor, dr. hab. Sławomir Szymański, not only for suggesting extremely interesting and intelectually challenging subject of this thesis, but also for his patience and continuous help.

The other person whose goodwill, hospitality and experience was priceless for me at the time of the hardest work is prof. Bernd Wrackmeyer from Bayreuth. I am truly grateful to him.

I would also like to thank prof. Lech Stefaniak for his friendship and generosity. He remains in my memory.

Finally, I wish to thank my family, my colleagues from the NMR group, and other friends of mine for creating a pleasant atmosphere and for their daily help.

Partial financial support from the Polish State Committee for Scientific Research (grant 3 T09A 06319) is gratefully acknowledged.

Contents

1 Introduction.

In NMR frequency table there are 118 magnetically active isotopes. Only 31 of these are spin-1/2 nuclei. The others have spin quantum number greater than 1/2 and therefore possess quadrupole moment. NMR spectroscopists measuring high resolution spectra in liquids usually try to avoid observing quadrupolar nuclei because nuclear spin relaxation of the latter, caused by quadrupolar coupling, is often very fast so that the spectral lines are substantially broadened. In many cases, the line broadening can be even so large that neither the chemical shift of nor the scalar coupling constants to the nucleus in question can be measured - if the signal acquisition can be correctly performed at all.

In my Ph.D. thesis, I shall show that in some cases fast nuclear quadrupolar relaxation is an underestimated source of invaluable information about molecular structure and dynamics, which cannot be obtained by other methods. My own research is focused on chemical compounds containing in their structure spin-1/2 nucleus, further referred to as a "spy" nucleus, scalar coupled to two isochronous nuclei of spin-1. The central element of these studies involves an identification and an interpretation of the effects, in the spectra of the spin-1/2 nucleus, of cross-correlations of fluctuating quadrupolar interactions of the spin-1 nuclei.

All of my own results to be reported in Chapter 3 involve molecules dissolved in non-viscous isotropic liquids. A brief exposition of the pertinent theoretical background to be presented in Chapter 2 is therefore confined to such a case.

2 Literature overview.

2.1 The physical origin of nuclear spin relaxation in isotropic fluids.

A general Hamiltonian of a nuclear spin system placed in an external static magnetic field of induction $\overrightarrow{B_0}$, directed along the z axis, reads (see, e.g., Ref. [1]):

$$\hat{H}(t) = \hat{H}_0 + \hat{H}_1(t) = \hbar \left(-\sum_i \omega_i \hat{I}_{zi} + 2\pi \sum_{i>j} J_{ij} \hat{\mathbf{I}}_i \hat{\mathbf{I}}_j \right) + \sum_\mu \hat{H}_{1\mu}(t), \quad (1)$$

where i and j label the nuclei, and index μ tags time-dependent, stochastically varying interactions in the spin system; $\hat{\mathbf{I}}_i$ is the spin operator of nucleus i, $\hat{I}_{zi}$ is the operator of z component of spin i. The first term in Eq. (1) describes Zeeman interactions which are responsible for Larmor precession of the nuclear spins in the magnetic field. The second term describes scalar couplings between the nuclei in the spin system, which are responsible for the fine structure of the resonance lines in NMR spectrum. The only time-dependent term in Eq. (1) is the last one. It varies in accord with stochastic molecular reorientation and its time-averaged value, $\langle \hat{H}_1(t) \rangle$, vanishes. Therefore, the index μ labels various orientation-dependent interactions such as those due to the chemical shift anisotropy, spin-rotation, nuclear quadrupole-electric field gradient and dipole-dipole[2]. It should be noted that each nucleus in a given spin system can be (and usually is) involved in more than one interaction. All the above enumerated interactions are a source of randomly varying perturbations of spin energy, which constitute a basis for the processes of nuclear spin relaxation. The return of an excited spin system back to thermal equilibrium is called T_1-type relaxation, and decay of coherences previously created in the sample (usually by application of radiofrequency pulses) is called T_2-type relaxation. The features of these time-dependent interactions leading to relaxation will be explained below on the example of the nuclear quadrupole-electric field gradient (EFG) [3] interaction.

As was mentioned above, the quadrupole moment is a property of the nuclei possessing spin quantum number greater than 1/2 (c.f., e.g. Ref. [4]). Its existence is a direct consequence of non-spherical internal charge distribution for nucleus of such a type. This is the reason why the energy of any such nucleus is dependent on its orientation relative to an external, non-uniform electric field. In a molecule, such a non-uniform field is generated mostly by the surrounding electronic cloud. For a single nucleus, the Hamiltonian of the

quadrupolar interaction in the laboratory reference frame is as follows [4]:

$$\begin{aligned}\hat{H}_{1Q} &= \frac{eQ}{4I(2I-1)}\left[\frac{2}{\sqrt{6}}V_0^{lab}(t)(3\hat{I}_z^2-\hat{\mathbf{I}}^2) - V_{+1}^{lab}(t)(\hat{I}_-\hat{I}_z+\hat{I}_z\hat{I}_-)\right. \\ &+ \left. V_{-1}^{lab}(t)(\hat{I}_+\hat{I}_z+\hat{I}_z\hat{I}_+) + V_{+2}^{lab}(t)(\hat{I}_-\hat{I}_-) + V_{-2}^{lab}(t)(\hat{I}_+\hat{I}_+)\right],\end{aligned} \tag{2}$$

where I is the spin quantum number, eQ is the quadrupole moment of the nucleus (in units of electron charge per m^2), and $\hat{I}_\pm = \hat{I}_x \pm i\hat{I}_y$, where $\hat{I}_x and \hat{I}_y$ are operators of the corresponding spin components. In Eq. (2), the symbols $V_0^{lab}, V_{\pm1}^{lab}, V_{\pm2}^{lab}$ denote components of a rank-2 irreducible spherical tensor describing the electric field gradient at the nuclear site. They can be expressed by the combinations of products of the Wigner rotation matrix elements $D^{(2)}_{(m,m')}$ and the EFG tensor components calculated in the system of its principal axes (pas) according to [1]:

$$V_m^{lab}(t) = \sum_{m'=-2}^{2} D^{(2)}_{(m,m')}(\Omega(t))V_{m'}^{pas} \tag{3}$$

where the set of the three Euler angles, $\Omega(t) = (\alpha(t), \beta(t), \gamma(t))$, describes an instantaneous orientation of the rapidly rotating molecule in the laboratory frame. The quantities $V_{m'}^{pas}$ can be directly defined by components of the corresponding Cartesian tensor, $\mathbf{C^{pas}}$, namely [1],

$$\begin{aligned}V_0^{pas} &= \frac{\sqrt{6}}{2}C_{zz}^{pas} \\ V_{\pm1}^{pas} &= \mp(C_{xz}^{pas} \pm iC_{zy}^{pas}) = 0 \\ V_{\pm2}^{pas} &= \frac{1}{2}(C_{xx}^{pas} - C_{yy}^{pas})\end{aligned} \tag{4}$$

where the principal axes of the tensor C are labelled according to the following convention [5]:

$$|C_{zz}^{pas}| \geqslant |C_{yy}^{pas}| \geqslant |C_{xx}^{pas}|. \tag{5}$$

Since C is a traceless tensor, it can be uniquely defined by its principal value, C_{zz}^{pas}, and asymmetry parameter

$$\eta = \frac{C_{xx}^{pas} - C_{yy}^{pas}}{C_{zz}^{pas}}, \quad 0 \leqslant \eta \leqslant 1. \tag{6}$$

Equation (3) shows explicitly that the time-dependence of the spherical tensor $\mathbf{V^{lab}}$ is carried solely by the elements of the Wigner rotation matrix. The elements $D^{(2)}_{(m,m')}$ are in turn time-dependent because they are functions of

the instantaneous Euler angles $\Omega(t)$. Equation (2) can be rewritten in a more compact form

$$\hat{H}_{1Q} = \frac{eQ}{4I(2I-1)} \sum_{m=-2}^{2} (-1)^m \hat{T}_m V_{-m}^{lab}(t) \tag{7}$$

in which the rank-2, irreducible spherical tensor spin operator of quadrupolar interaction, $\hat{\mathbf{T}}$, is defined as follows:

$$\begin{aligned} \hat{T}_0 &= \frac{1}{\sqrt{6}}[3\hat{I}_z^2 - I(I+1)] \\ \hat{T}_{\pm 1} &= \mp(\hat{I}_z\hat{I}_\pm + \hat{I}_\pm\hat{I}_z) \\ \hat{T}_{\pm 2} &= \hat{I}_\pm^2. \end{aligned} \tag{8}$$

In cases where the random molecular reorientations are rapid compared to the energy of quadrupolar interaction,

$$E_Q = \frac{e^2 Q V_0^{pas}}{4I(2I-1)}, \tag{9}$$

expressed in units of angular frequency, the traceless tensor $\mathbf{V^{lab}}$ is averaged out to zero. Nevertheless, from the point of view of nuclear spin, rapid changes of the orientation of the latter, may cause transition between Zeeman energy levels and, therefore, both T_1 and T_2-type relaxation.

2.2 An outline of Bloch–Wangsness–Redfield (BWR) relaxation theory. [6, 7]

In presence of nuclear spin relaxation, the spin states of individual molecules in the sample cannot be specified. The system as a whole can be treated as a statistical mixture of states ψ_n which form a complete orthonormal basis in the spin space of a single molecule. The state of such a system is described in terms of spin density operator, $\hat{\rho}$, which is defined as follows [8]:

$$\hat{\rho} = \sum_n W_n |\psi_n\rangle\langle\psi_n|, \tag{10}$$

where W_n is the probability of finding a molecular spin system in state ψ_n. A knowledge of the density operator and its evolution in time, governed by the Liouville–von Neumann equation [8]

$$\frac{d\hat{\rho}}{dt} = -\frac{i}{\hbar}[\hat{H}(t), \hat{\rho}], \tag{11}$$

is sufficient for an exact description of the behaviour of the investigated sample in any NMR experiment. Unfortunately, because of its stochastic character, time-dependence of the Hamiltonian entering right-hand side of Eq. (11) cannot be specified exactly. Therefore, this equation cannot be solved accurately, and approximate methods of statistical quantum mechanics must be applied.

It is convenient to represent the above equation in Liouville space [9, 10, 11] in which density matrix $\hat{\rho}$ becomes a column vector $|\rho\rangle$ and the commutator with the spin Hamiltonian $\hat{H}(t)$ is replaced by the Liouville derivation superoperator[†] $\mathbf{L}(t) \equiv \frac{1}{\hbar}\hat{H}(t)^D = \frac{1}{\hbar}(\hat{H}(t) \otimes \hat{1} - \hat{1} \otimes \hat{H}(t)^*)$, where the symbol "$\otimes$" denotes a Kronecker product of the corresponding matrices, thus,

$$\frac{d|\rho\rangle}{dt} = -i\mathbf{L}(t)|\rho\rangle. \tag{12}$$

The fact that time-dependent part, $\hat{H}_1(t)$, of the Hamiltonian described in Eq. (1) is much smaller than its time-independent part, $\hat{H}_0$, allows one to solve Eq. (12) approximately by applying perturbation calculus of second order to its modified version obtained by transformation to the so-called interaction representation. On back transformation to the Schrödinger representation, and upon putting $\mathbf{L} = \frac{1}{\hbar}(\hat{H}_0 \otimes \hat{1} - \hat{1} \otimes \hat{H}_0^*)$, one obtains the BWR equation of motion

$$\frac{d|\rho\rangle}{dt} = -i\mathbf{L}|\rho\rangle + \mathbf{R}(|\rho\rangle - |\rho_0\rangle), \tag{13}$$

where

$$\hat{\rho}_0 = \frac{\exp(-\frac{\hbar\hat{H}_0}{k_B T})}{Tr\left[\exp(-\frac{\hbar\hat{H}_0}{k_B T})\right]} \tag{14}$$

is the thermal equilibrium density operator, with Tr denoting the trace of an operator.

Equation (13) is the central result of the BWR relaxation theory [6, 7]. As can be seen from it, the relaxation superoperator $\mathbf{R}$ acts only on non-equilibrium density vector, causing return of the excited system back to thermal equilibrium with the reservoir. When the system is already in equilibrium with the bath, i.e., when its state is described by the vector $|\rho_0\rangle$, then the term $\mathbf{R}(|\rho\rangle - |\rho_0\rangle)$ vanishes, and in absence of any external radiofrequency fields, the evolution of the system is stopped.

Equation (13) is valid only in the so-called extreme narrowing condition, i.e. when both an average correlation time τ_c of the molecule and Larmor

[†]Any operator $\hat{O}$ in Hilbert space can be derivated. The result of this transformation is the superoperator $\hat{O}^D \equiv \hat{O} \otimes \hat{1} - \hat{1} \otimes \hat{O}^*$ in Liouville space.

frequency ω_0 of the observed nucleus fulfil the inequality $\tau_c \ll 1/\omega_0$, which is a common case for medium size and small molecules in non-viscous isotropic fluids. Beyond this regime, some additional effects are non-negligible and must be taken into account, which makes Eq. (13) more complicated.

In Eq. (13), the superoperator $\mathbf{R}$ has the following form [11]

$$\mathbf{R} = -\sum_{\mu \leqslant \mu'} \mathbf{R}_{\mu\mu'} \tag{15}$$

with the auto-correlation and the cross-correlation contributions to relaxation being described by

$$\mathbf{R}_{\mu\mu} = J_{\mu\mu} \sum_{m=\lambda}^{-\lambda} (-1)^m \hat{T}^D_{\mu m} \hat{T}^D_{\mu -m} \tag{16a}$$

and

$$\mathbf{R}_{\mu\mu'} = J_{\mu\mu'} \delta_{\lambda\lambda'} \sum_{m=\lambda}^{-\lambda} (-1)^m \left[\hat{T}^D_{\mu m} \hat{T}^D_{\mu' -m} + \hat{T}^D_{\mu' -m} \hat{T}^D_{\mu m} \right], \tag{16b}$$

respectively, where λ is the rank of the irreducible spherical tensor spin operators, $\hat{\mathbf{T}}$, of the corresponding interactions μ and μ'. The spectral densities $J_{\mu\mu'}$ are integrals

$$J_{\mu\mu'} = \int_0^\infty C_{\mu\mu'}(\tau) d\tau \tag{17}$$

of the ensemble-averaged time correlation functions $C_{\mu\mu'}(\tau)$ of the corresponding time-dependent functions entering Eq. (2). In Eq. (16b), apart from the simplification resulting from the extreme narrowing approximation, two more properties of the system are exploited:(i) axial symmetry of the system with respect to rotations around z axis of the laboratory frame (which is parallel to the direction of external magnetic field), and (ii) the lack of any orientational anisotropy of the molecules forming an isotropic fluid. From property (i) it follows that in Eq. (16b) pairs of spherical tensor components superoperators $\hat{T}^D_{\mu m}$ and $\hat{T}^D_{\mu' m'}$ where $m' \neq -m$ are absent. Hence, the only correlation functions that are of relevance are those between the corresponding time dependent functions $V^{lab}_{\mu -m}$ and $V^{lab}_{\mu' m}$ (c.f. Eqs. (2) and (7)). By virtue of property (ii), contributions to relaxation from pairs of time-dependent interactions described by tensors of different ranks vanish [12]. Moreover, for any pairs of interactions μ and μ' (of the same rank λ), the correlation functions are independent of m [12]. Therefore, in calculating the relevant correlation functions,

one can confine oneself to the $m = 0$ components defined in Eq. (3). For rank-2 interactions μ and μ' one therefore has [13]

$$C_{\mu\mu'}(\tau) = \sum_{k=-2}^{2} \sum_{l=-2}^{2} \left\langle D^{(2)}_{(0,k)}(\Omega_\mu(t)) D^{(2)*}_{(0,l)}(\Omega_{\mu'}(t+\tau)) \right\rangle V^{pas}_{\mu k} V^{pas}_{\mu' l}, \tag{18a}$$

where $\Omega_\mu(t)$ describes orientation in the laboratory frame of the principal axis system of tensor $\mathbf{V}^{\mathbf{pas}}_{\mu}$ at instant t while $\Omega_{\mu'}(t+\tau)$ does the same for tensor $\mathbf{V}^{\mathbf{pas}}_{\mu'}$ at instant $t+\tau$. Equation (18a) is valid for any rank-2 tensors $\mathbf{V}^{\mathbf{pas}}_{\mu}$ and $\mathbf{V}^{\mathbf{pas}}_{\mu'}$. If asymmetry parameters η and η' of both such tensors are equal to zero, Eq. (18a) can be rewritten as follows:

$$C_{\mu\mu'}(\tau) = \left\langle D^{(2)}_{(0,0)}(\Omega_\mu(t)) D^{(2)}_{(0,0)}(\Omega_{\mu'}(t+\tau)) \right\rangle V^{pas}_{\mu 0} V^{pas}_{\mu' 0}. \tag{18b}$$

In the latter case, auto- and cross-correlation spectral density functions can be derived easily, whenever both the motional model and the geometry of the molecule are known. In the case of non-axially symmetric tensors, calculations of the spectral densities in question can also be performed. However, doing this in the standard way requires an extensive use of Wigner rotation matrices, which is inconvenient. In such a case, following a method proposed by Werbelow [14], any traceless Cartesian tensor $\mathbf{C}$, referred to its own principal axis system, can be decomposed into two traceless tensors $\mathbf{C}'_{\mathbf{z}}$ and $\mathbf{C}'_{\mathbf{x}}$ both having axial symmetry, but with respect to the z and x axes, respectively, of the original tensor, namely,

$$\mathbf{C} = \mathbf{C}'_{\mathbf{z}} + \mathbf{C}''_{\mathbf{x}}, \tag{19}$$

where

$$\mathbf{C}'_{\mathbf{z}} = \begin{bmatrix} -\frac{1}{3}\Delta C' & 0 & 0 \\ 0 & -\frac{1}{3}\Delta C' & 0 \\ 0 & 0 & \frac{2}{3}\Delta C' \end{bmatrix} \tag{20a}$$

and

$$\mathbf{C}''_{\mathbf{x}} = \begin{bmatrix} \frac{2}{3}\Delta C'' & 0 & 0 \\ 0 & -\frac{1}{3}\Delta C'' & 0 \\ 0 & 0 & -\frac{1}{3}\Delta C'' \end{bmatrix}, \tag{20b}$$

with

$$\begin{aligned} \Delta C' &= C^{pas}_{zz} - C^{pas}_{yy} \\ \Delta C'' &= C^{pas}_{xx} - C^{pas}_{yy}. \end{aligned} \tag{21}$$

Now, the auto-correlation function for an axially non-symmetric interaction tensor will be given by a sum of two auto-correlation functions for its respective axially symmetric components plus twice the cross-correlation function between the latter. Accordingly, the corresponding spectral density will be given by [14, 15]:

$$J_{CC} = J_{C'_z C'_z} + J_{C''_x C''_x} + 2J_{C'_z C''_x}. \tag{22}$$

Similarly, the cross-correlation spectral density for two traceless axially non-symmetric interaction tensors **C** and **D** will be given by [14, 15]:

$$J_{CD} = J_{C'_z D'_z} + J_{C''_x D''_x} + J_{C'_z D''_x} + J_{C''_x D'_z}. \tag{23}$$

In what follows, individual axially symmetric components of the interaction tensors will be treated as distinct interactions and, accordingly, will be denoted by different labels μ, μ' etc. This will not lead to ambiguities. Details concerning practical calculations of both auto- and cross-correlation spectral densities involving two axially symmetric tensors will be discussed in the next chapter.

2.3 Spectral densities and motional models.

In the right-hand side of Eq. (18b), an ensemble-averaged product of elements of Wigner rotation matrices appears. The form in which it is written is inconvenient for practical applications since its dependences on both the rotational diffusion process and on the molecular geometry parameters are not evident. Therefore, the term $\langle D^{(2)}_{(0,0)}(\Omega_\mu(t)) D^{(2)}_{(0,0)} \Omega_{\mu'}(t+\tau))\rangle$ is normally evaluated in the context of an appropriate diffusional rotation model in order to derive its explicit dependence on the parameters of molecular structure and dynamics. One of the central points of such an evaluation is the solution of the rotational diffusion equation. For this purpose, both the irreducible spherical tensors $\mathbf{V}^{\mathbf{pas}}_{\mu}$ and $\mathbf{V}^{\mathbf{pas}}_{\mu'}$ entering Eq. (18b) are to be first expressed in the system of principal axes of the rotational diffusion tensor which is the most natural reference frame in the case discussed currently. This is done by simple transformations, mathematically expressed in terms of multiplications of $\mathbf{V}^{\mathbf{pas}}_{\mu}$ and $\mathbf{V}^{\mathbf{pas}}_{\mu'}$ by appropriate elements of Wigner rotation matrice. The latter are defined by the Eulerian angles referring the principal axes of $\mathbf{V}_\mu$ and $\mathbf{V}_{\mu'}$ to the principal axes of the diffusion tensor of the molecule. After these preliminary transformations, the close analogy between the rotational diffusion equation and the Schrödinger equation for the free rotor can be exploited [16, 17]; this provides a convenient way to solve the former. Finally, one obtains formulas in which auto- and cross-correlation [18, 19, 20] spectral

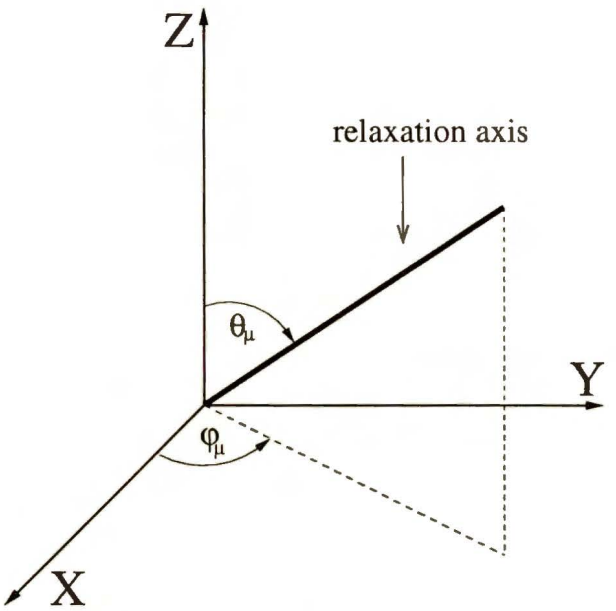

Figure 1: Definition of the polar angles θ_μ and φ_μ of the relaxation axis μ with respect to the principal axes X, Y, and Z of the diffusion tensor.

densities are expressed as functions of three diffusion coefficients D_X, D_Y, and D_Z describing the molecular motions about X, Y, and Z principal axes of the diffusion tensor, respectively, and of two polar angles θ_μ and φ_μ (see Fig. 1) for each of the interaction tensors involved [17]. These angles define orientations of the unique symmetry axis ("relaxation axis") of the given (axially symmetric, see comment following Eq. (23)) interaction tensor in the principal system of the diffusion tensor.

$$J_{\mu\mu'}(\omega) = \sum_{m=-2}^{2} a_m \frac{(2/\lambda_m)}{1+\omega^2/\lambda_m^2} \tag{24}$$

where

$$\begin{aligned} \lambda_0 &= 4D_Z + 2D_+ \\ \lambda_{\pm 1} &= D_Z + 5D_+ \pm 3D_- \\ \lambda_{\pm 2} &= 2D_Z + 4D_+ \pm [4(D_Z - D_+)^2 + 12D_-^2]^{1/2} \end{aligned} \tag{25}$$

and

$$\begin{aligned} a_0 &= (3/4)\sin^2\theta_\mu \sin^2\theta_{\mu'} \sin 2\varphi_\mu \sin 2\varphi_{\mu'} \\ a_{+1} &= (3/4)\sin 2\theta_\mu \sin 2\theta_{\mu'} \sin\varphi_\mu \sin\varphi_{\mu'} \end{aligned}$$

$$
\begin{aligned}
a_{-1} &= (3/4)\sin 2\theta_\mu \sin 2\theta_{\mu'} \cos\varphi_\mu \cos\varphi_{\mu'} \\
a_{\pm 2} &= \frac{1}{12D_-^2 + d_\pm^2}\left\{(9D_-^2)\sin^2\theta_\mu \cos 2\varphi_\mu \sin^2\theta_{\mu'} \cos 2\varphi_{\mu'}\right. \\
&- (3D_- d_\pm)[\sin^2\theta_\mu \cos 2\varphi_\mu (1/2)(3\cos^2\theta_{\mu'} - 1) \\
&+ (1/2)(3\cos^2\theta_\mu - 1)\sin^2\theta_{\mu'} \cos 2\varphi_{\mu'}] \\
&+ \left.(d_\pm^2(1/2)(3\cos^2\theta_\mu - 1)(1/2)(3\cos^2\theta_{\mu'} - 1)\right\}
\end{aligned}
\tag{26}
$$

with

$$
\begin{aligned}
D_\pm &= (D_X \pm D_y)/2 \\
d_\pm &= 2(D_Z - D_+) \mp \left[4(D_Z - D_+)^2 + 12D_-^2\right]^{1/2}
\end{aligned}
$$

Equation (24) is valid for a general case in which all the three diffusion coefficients are not equal to one another, i.e., $D_X \neq D_Y \neq D_Z$ [20]. It is quite a common case where the tensor of rotational diffusion is axially symmetric, i.e., $D_X = D_Y \neq D_Z$. Then, defining effective correlation times τ_{20}, τ_{21}, and τ_{22} according to

$$
\begin{aligned}
1/\tau_{20} &= 6D_X \\
1/\tau_{21} &= 5D_X + D_Z \\
1/\tau_{22} &= 2D_X + 4D_Z,
\end{aligned}
\tag{27}
$$

one can replace Eq. (24) by the following one:

$$
\begin{aligned}
J_{\mu\mu'}(\omega) &= (1/2)(3\cos^2\theta_\mu - 1)(1/2)(3\cos^2\theta_{\mu'} - 1)\frac{2\tau_{20}}{1+\omega^2\tau_{20}^2} \\
&+ (3/4)\sin(2\theta_\mu)\sin(\theta_{\mu'})\cos(\varphi_\mu - \varphi_{\mu'})\frac{2\tau_{21}}{1+\omega^2\tau_{21}^2} \\
&+ (3/4)\sin^2\theta_\mu \sin^2\theta_{\mu'} \cos 2(\varphi_\mu - \varphi_{\mu'})\frac{2\tau_{22}}{1+\omega^2\tau_{22}^2}.
\end{aligned}
\tag{28}
$$

Finally, in the simplest case where the molecule undergoes an isotropic reorientation, i.e. $D_X = D_Y = D_Z = D$, the corresponding spectral densities are expressed by the formula:

$$
J_{\mu\mu'}(\omega) = (1/2)(3\cos^2\alpha - 1)\frac{2\tau_c}{1+\omega^2\tau_c^2},
\tag{29}
$$

where α is the angle between the two relevant relaxation axes, and $\tau_c = 1/6D$ is an average correlation time for the whole molecule.

Spectral densities in Eqs. (24), (28) and (29) are formally functions of ω. Dependence on the latter variable is obviously negligible when the condition of extreme narrowing (i.e., $\omega\tau \ll 1$) is fulfilled.

2.4 Experimental observation of cross-correlation spectral densities for quadrupolar interactions.

The first attempt at experimental determination of cross-correlation spectral densities for two quadrupole interactions, preceeded by careful theoretical considerations, was reported in 1980 by Vold et al.[21, 22] for a solution of deuterated dichloromethane CD_2Cl_2 in a nematic liquid crystal solvent. At variance with the situation in isotropic liquids, which is describable by the formalism of the preceeding sections, in such an oriented phase, the deuteron relaxation in a CD_2 group is described by six different spectral densities: three auto-correlation terms, $J_0^A(0)$, $J_1^A(\omega_0)$, and $J_2^A(2\omega_0)$, which characterize the motion of the EFG tensor of either deuteron; and three cross-correlation terms, $J_0^C(0)$, $J_1^C(\omega_0)$, and $J_2^C(2\omega_0)$, which describe cross-correlation between the motions of the two tensors. This is because relaxation of the deuterons of CD_2 group is governed not only by the reorientation of the dichloromethane molecule itself, but also by coherent fluctuations of the nematic director [23]. These fluctuations are slow and as such they render the extreme narrowing condition inapplicable. In order to determine all of these parameters, the authors applied non-selective and semiselective inversion-recovery experiments, as well as two-dimensional Fourier transform techniques allowing for measurements of transverse decays of both single-quantum and double-quantum spin-echoes. It should be emphasized that the existence of the partial order introduced by the presence of the liquid crystal molecules is a necessary condition of applicability of these experimental methods. Such methods cannot be successfully applied in studies of molecular motion in an isotropic phase, in which both the quadrupolar and dipolar coupling constants do not manifest themselves as resolved line splittings of sufficiently large magnitudes. From the above spectral densities, the anisotropy of reorientation of the investigated molecule was estimated to be between 10 and 30. These results are rather qualitative than quantitative and concern the molecular motion in a specific environment created by the liquid crystal surrounding.

Recently, Werbelow et al. [24] observed a manifestation of the quadrupolar cross-correlation in NMR spectrum of a spin-1/2 nucleus coupled to a system of two spin-1 isochronous nuclei. In the regime of slow quadrupolar relaxation, in the ^{13}C multiplets of deuterated ethylene glycol, it was observed that, due to differential line broadenings, the heights of the multiplet components do not fit the simple pentet pattern. These effects were explained in terms of BWR theory as being due to both auto- and cross-correlation effects between the two quadrupolar interactions. Unfortunately, because of an incorrect theoretical description of the investigated spectra ignoring an earlier analysis of

the problem [25], the results presented in the work [24] must be disqualified. As the correct expressions for the corresponding signals are derived by myself, further detailed discussion of the work of Werbelow et al. [24] is carried out in the part presenting my own results.

3 Results and discussion.

The bulk of literature data documenting usefulness of nuclear spin relaxation phenomena for structural studies in solutions involves the dipolar relaxation mechanism. This is due to an explicit dependence of the dipolar relaxation rates on the internuclear distances. Relaxation mechanisms arising from fluctuating interactions that engage single nuclei, such as nuclear quadrupole - electric field gradient and nuclear dipole - external magnetic field modulated by chemical shift anisotropy (CSA), may seem to be of limited interest in this context because of a lack of any straightforward dependence on the intramolecular distances. However, as was already emphasized that randomly modulated interactions of any sort that lead to relaxation can interfere with one another to produce the cross-correlation contributions to relaxation. Cross-correlations may even arise between interactions that operate in remote parts of the molecule. Thus, despite the fact that they still do not bear any functional dependence on the distances, in some cases they may provide crucial structural information. According to a recent review on the cross-correlation effects [26], in the past the research was predominantly concentrated on the instances where the cross-correlated interactions share one nucleus in common; cross-correlation of fluctuating dipolar coupling between a ^{13}C nucleus and an adjacent proton, and fluctuating, CSA-mediated interaction of the former is a typical example. Little attention was devoted to cross-correlation effects in systems of quadrupolar nuclei interacting with the EFG's. To the best of my knowledge, the only papers devoted to this problem are those reviewed in Section 2.4. The methods of evaluation of such effects that were once developed by Vold et al.[21, 22], which involve partially ordered systems exhibiting resolved quadrupolar splittings, were briefly reviewed in Section 2.4. For isotropic fluids, where such splittings do not occur, an appropriate general methodology has not been worked out yet. Elaboration of such a methodology was one of main goals of my Ph.D. thesis. In the present chapter, on the example of several molecular systems, I shall show that accurate, quantitative determination of quadrupolar cross-correlations and a careful analysis thereof in connection to other spectral parameters (e.g. relaxation times) can provide a new insight into molecular structure and dynamics in isotropic liquids.

As I mention in the Introduction, my experimental results involve compounds containing in their structure a nucleus whose T_1-relaxation is relatively slow, preferably a spin-1/2 nucleus, scalar coupled to two isochronous nuclei of spin-1 (i.e., quadrupolar nuclei). NMR signal of such a spy nucleus is in a characteristic way dependent on quadrupolar cross-correlation between the isochronous nuclei [25] provided that the quadrupolar relaxation rates are

not prohibitively fast compared with the J-coupling between the latter and the spy nucleus. Spectra of such compounds dissolved in non-viscous isotropic solvents were numerically analysed by me using iterative computer programs written by Szymański [27]. These programs are based on the BWR relaxation theory, briefly described in preceeding chapter. The "best fit" theoretical spectra, in the least-squares sense, are obtained by varying the parameters, which are the experimental spectra dependent on, according to the Gauss-Newton minimisation scheme. Unfortunately, the numerical results obtained using a general computer routine, although perfectly correct, do not provide full insight into the physics of the investigated problem. Therefore at the beginning of this part of my thesis, I am in a duty to derive explicit formulae describing the spin systems of central interest in the present work, using an appropriate spin basis. This affords a deeper interpretation of the investigated phenomena. As I have already mentioned in Section 2.4, in the literature I have found a paper which addresses the above problem under some limiting conditions, but does this in an incorrect way [24]. I shall perform a detailed discussion of that paper and argue those of its points the inaccuracy of which leads to significant, systematic errors in determination of the parameters that are of central significance for my research, i.e., the quadrupolar cross-correlation spectral densities. Then I consider two experimental examples, some aspects of which are of theoretical and/or practical importance for the determination of the latter parameters. Finally, the methodology elaborated in the above studies I apply to the problem of solution structure of bis(hexamethyldisilylamido)-mercury(II).

Some of the results described in this chapter were already published [28, 29].

3.1 Theoretical description of NMR spectra of spin-1/2 nucleus scalar coupled to two equivalent, spin-1 nuclei.

3.1.1 The limit of slow quadrupolar relaxation.

The spectrum of spin-1/2 nucleus scalar coupled to a group of magnetically equivalent nuclei of spin>1/2, besides being dependent on quadrupolar cross-correlation between such nuclei, can also be dependent on the scalar couplings between the latter [25]. Such a disturbance of magnetic equivalence can be predicted from BWR theory when spin relaxation of the equivalent nuclei is non-negligible. When the values of the coupling constants between such nuclei are unknown, effects of a broken magnetic equivalence may be a source of

systematic distortions in a quantitative analysis of the spectra. In a study on quadrupolar cross-correlation in a $^{13}CD_2$ spin system, Werbelow et al. [24] reported an approximate, closed-form expression for the lineshape of the spin-1/2 nucleus for the limiting case where quadrupolar relaxation rates of the equivalent spin-1 nuclei are small in comparison with the heteronuclear J-coupling constant, in which instance the ^{13}C pentet remains well-resolved. However, such a simplification was achieved by the authors cited at the cost of a neglect of the possible effects of the disturbed magnetic equivalence on the lineshape. In this part of my thesis, I specify the range of validity of the above approximation and identify the instances where it fails in the description of resolved spectra of a general AX_2 ($I_A = 1/2$, $I_X = 1$). I also present explicit expressions for the elements of the matrix entering complete lineshape equation, which is valid not only for slow quadrupolar relaxation limit but for any relaxation rates (however, as long as the extreme narrowing condition is fulfilled). The discussion involves the case where relaxation mechanisms other than quadrupolar can be neglected in the description of spin dynamics of subsystem X_2 in the zero-quantum manifold, which is the only relevant one for a description of the spectrum of part A (double resonance experiments will not be considered in the present work).

Elements of the Hilbert space basis for X_2 subsystem, which are used in the following considerations, are listed in Table 3.1. Each state of X_2 can be associated with one of the two basic states of spin A, α and β. This gives 9 vectors $|\alpha\rangle|SM\rangle$ and 9 vectors $|\beta\rangle|SM\rangle$, where $|\alpha\rangle$ and $|\beta\rangle$ are eigenvectors of $\hat{I}_z$ operator of spin A, and $|SM\rangle$ are simultaneous eigenvectors of the squared total X-spin, $\hat{\mathbf{S}}^2 = (\hat{\mathbf{S}}_1 + \hat{\mathbf{S}}_2)^2$, and total X-spin z-component, $\hat{S}_z = \hat{S}_{z1} + \hat{S}_{z2}$, operators, concerned with eigenvalues $S(S+1)(S = 0, 1, 2)$, and $M = -2S, -2S+1, \ldots, 2S$, respectively. The vectors $|\gamma\rangle|1M\rangle$ are antisymmetric while those $|\gamma\rangle|2M\rangle$ and $|\gamma\rangle|0M\rangle$ are symmetric under permutation of the X nuclei. In the framework of BWR theory, single quantum spectra of nucleus A can be described in terms of time evolution of 11 coherences represented by the superkets $|I_+\rangle|SMS'M\rangle$, where $|I_+\rangle \equiv |\alpha\rangle\langle\beta|$, and $|SMS'M\rangle \equiv |SM\rangle\langle S'M|$, with $|S - S'|$ being equal to either 0 or 2. The coherences for which $|S - S'| = 1$ involve spin states of different permutation symmetries so that, by virtue of macroscopic conservation of nuclear permutation symmetry, they remain uncoupled from those involving states of the same permutation symmetry and effects of their possible occurence are never observed [11]. For any relaxation rates, the spectra of A can thus be described in terms of a 11×11 spectral matrix $\mathbf{W}$ presented in the Table 3.2. Its real part comprises the zero-quantum symmetric block of the BWR quadrupolar relaxation matrix, with the diagonal elements augmented by rate constant

Table 3.1: Spin state basis set for X_2 subsystem. Definitions of quantum numbers S and M are given in the text.

Label	Description in terms of product states	$\|SM\rangle$
$\|1\rangle$	$\|11\rangle$	$\|22\rangle$
$\|2\rangle$	$(\|10\rangle + \|01\rangle)/\sqrt{2}$	$\|21\rangle$
$\|3\rangle$	$(\|10\rangle - \|01\rangle)/\sqrt{2}$	$\|11\rangle$
$\|4\rangle$	$(\|1\,{-1}\rangle + \|\,{-11}\rangle + 2\|00\rangle)/\sqrt{6}$	$\|20\rangle$
$\|5\rangle$	$(\|1\,{-1}\rangle - \|\,{-11}\rangle)/\sqrt{2}$	$\|10\rangle$
$\|6\rangle$	$(\|1\,{-1}\rangle + \|\,{-11}\rangle - \|00\rangle)/\sqrt{3}$	$\|00\rangle$
$\|7\rangle$	$(\|\,{-10}\rangle - \|0\,{-1}\rangle)/\sqrt{2}$	$\|1\,{-1}\rangle$
$\|8\rangle$	$(\|\,{-10}\rangle + \|0\,{-1}\rangle)/\sqrt{2}$	$\|2\,{-1}\rangle$
$\|9\rangle$	$\|\,{-1}\,{-1}\rangle$	$\|2\,{-2}\rangle$

$w = 1/T_2^*$ which describes an accumulated effect of all 'extraneous' factors that contribute to line broadenings in the spectra of A (e.g. external magnetic field inhomogeneity). The imaginary part is a diagonal matrix. Nine of its elements, those concerned with the superkets $|I_+\rangle|SMSM\rangle$, describe the individual frequencies of the A pentet, $-i(\omega_{0A} + 2\pi M J_{AX}$; for $|M| = 0$ and 1 these elements are three- and two-fold degenerate, respectively. The corresponding coherences, violating conservation of total spin of the X_2 subsystem, were once termed 'partly allowed coherences' because for negligible relaxation they are factored out of the remaining, 'fully allowed' coherences and become undetectable by the NMR receiver coil: as opposite to the latter, the former do not contribute to observable magnetization [25]. Nevertheless, even in the limit of slow relaxation, i.e when

$$2\pi|J_{AX}| \gg 1/T_{1Q} \geqslant w, \tag{30}$$

they can modulate the behaviour of the nine 'magnetic' coherences via the corresponding off-diagonal elements of the BWR quadrupolar relaxation matrix. The influence of such a modulation on NMR spectra of A can be particularly

Table 3.2: Elements of spectral matrix **W** describing lineshape of part A of the AX_2 spin system of the text; j and k denote auto- and cross-correlation spectral densities, respectively; $20j = 1/T_{1Q}$, $w = 1/T_2^*$, $\Delta\omega = \omega_{0A} - \omega$, $a = 2\pi|J_{AX}|$, and $x = 2\pi|J_{XX}|$.

$\|1\rangle\langle 1\|$	$\|2\rangle\langle 2\|$	$\|3\rangle\langle 3\|$	$\|4\rangle\langle 4\|$	$\|5\rangle\langle 5\|$	$\|6\rangle\langle 6\|$	$\|7\rangle\langle 7\|$	$\|8\rangle\langle 8\|$	$\|9\rangle\langle 9\|$	$\|4\rangle\langle 6\|$	$\|6\rangle\langle 4\|$
$i(\Delta\omega+2a)+$ $w+24j$	$-4(j+k)$	$-4(j-k)$	$-\frac{8}{3}(j+k)$	$-8(j-k)$	$-\frac{16}{3}(j+k)$	0	0	0	$-\frac{8\sqrt{2}}{3}(j+k)$	$-\frac{8\sqrt{2}}{3}(j+k)$
	$i(\Delta\omega+a)+$ $w+26j+2k$	$-6(j-k)$	$-\frac{2}{3}(j+k)$	$-2(j-k)$	$-\frac{16}{3}(j+k)$	$-4(j-k)$	$-4(j+k)$	0	$\frac{16\sqrt{2}}{3}(j+k)$	$\frac{16\sqrt{2}}{3}(j+k)$
		$i(\Delta\omega+a)+$ $w+26j-14k$	$-6(j-k)$	$-2(j+k)$	0	$-4(j+k)$	$-4(j-k)$	0	0	0
			$i\Delta\omega+w+$ $24j$	0	$-\frac{16}{3}(j+k)$	$-6(j-k)$	$-\frac{16}{3}(j+k)$	$-\frac{16}{3}(j+k)$	$\frac{8\sqrt{2}}{3}(j+k)$	$\frac{8\sqrt{2}}{3}(j+k)$
				$i\Delta\omega+w+$ $24j-16k$	0	$-2(j+k)$	$-2(j-k)$	$-8(j-k)$	0	0
					$i\Delta\omega+w+$ $\frac{80}{3}(j+k)$	0	$-\frac{2}{3}(j+k)$	$-\frac{8}{3}(j+k)$	0	0
						$i(\Delta\omega-a)+$ $w+26j-14k$	$-6(j-k)$	$-4(j-k)$	0	0
							$i(\Delta\omega-a)+$ $w+26j+2k$	$-4(j+k)$	$\frac{16\sqrt{2}}{3}(j+k)$	$\frac{16\sqrt{2}}{3}(j+k)$
								$i(\Delta\omega-2a)+$ $w+24j$	$-\frac{8\sqrt{2}}{3}(j+k)$	$-\frac{8\sqrt{2}}{3}(j+k)$
									$i(\Delta\omega+3x)+$ $w+\frac{80}{3}j+\frac{44}{3}k$	$-\frac{16}{3}(j+k)$
										$i(\Delta\omega-3x)+$ $w+\frac{80}{3}j+\frac{44}{3}k$

large in the limit of moderate relaxation, defined by the inequalities

$$2\pi|J_{AX}| \cong 1/T_{1Q} \gg w, \tag{31}$$

because in such a case the magnitudes of the corresponding off-diagonal elements of the matrix **W** will in general become comparable with the differences between the diagonal elements. Only in the situation (probably seldom occuring in practice) where $|J_{XX}| \gg |J_{AX}|$ can the non-magnetic coherences (those in the last two columns in Table 3.2) be generally discarded. On the other hand, for slow relaxation, such effects can be non-negligible only when the frequencies of these offending coherences happen to coincide, to withing a few quadrupolar relaxation rate constants, with those of the individual magnetic coherences. If there are no such coincidencies, in a description of the spectra of A one can retain only the 9×9 block of the spectral matrix, comprising only the nine magnetic coherences. In view of Eq. (30), this retained part undergoes a further approximate factoring into independent subblocks according to the degeneration pattern of its imaginary (diagonal) elements: each of the outer components of the pentet will then be described by a 1×1 subblock, each of the two inner components by a 2×2 subblock, and the central component by a 3×3 subblock. Such a factorization is obviously not possible in the limit specified in Eq. (31) because then the relaxation couples all the components of the pentet to form one poorly structured cluster.

In the limit of slow quadrupolar relaxation (Eq. (30)), which was of interest for Werbelow et al. [24], these authors found the above mentioned 3×3 subblock to be further factored into 1×1 and 2×2 sub-subblocks, which allowed these authors to derive closed-form lineshape expressions for each of the individual components of the pentet in the limit of slow quadrupolar relaxation. Below I give the corresponding lineshape equations, in matrix form, in the instances where the frequencies of the non-magnetic coherences coincide with the frequencies of (i) the outer components, (ii) the inner components, and (iii) the central component. In writting down the lineshape formulae involved I exploit the fact that the spectra of the system considered are independent on the absolute and relative signs of J_{AX} and J_{XX}. In these equations the quantities $2\pi|J_{AX}|$ and $2\pi|J_{XX}|$ are denoted a and x, respectively, and the quantity $\omega_{0A} - \omega$ by $\Delta\omega$. The quadrupolar auto- and cross-correlation spectral densities, j and k, respectively, expressed in rad s^{-1} are calibrated according to Ref. [30], so that $20j = 1/T_{1Q}$. The same convention is also used for the expressions in Table 3.2. The spectral submatrices relevant in the slow relaxation limit of Eq. (30), listed below, contain explicit expressions for all of the BWR relaxation matrix elements which in the full 11×11 spectral matrix describe couplings between the two non-magnetic and nine magnetic coherences.

Thus, in case (i), each of the outer components will be described by the equation

$$Y_o(\omega) = \begin{bmatrix} 1 & 0 \end{bmatrix} \times \begin{bmatrix} i(\Delta\omega \pm 2a) + w + 24j & -\frac{8\sqrt{2}}{3}(j+k) \\ -\frac{8\sqrt{2}}{3}(j+k) & i(\Delta\omega \pm 3x) + w + \frac{(80j+44k)}{3} \end{bmatrix}^{-1} \times \begin{bmatrix} 1 \\ 0 \end{bmatrix}. \quad (32)$$

In the case (ii), the corresponding equation for each of the inner components reads:

$$-Y_i(\omega) = \begin{bmatrix} 1 & 1 & 0 \end{bmatrix} \times \begin{bmatrix} i(\Delta\omega \pm a) + w + 26j + 2k & -6(j-k) & -\frac{4\sqrt{2}}{3}(j+k) \\ -6(j-k) & i(\Delta\omega \pm a) + w + 26j - 14k & 0 \\ -\frac{4\sqrt{2}}{3}(j+k) & 0 & i(\Delta\omega \pm 3x) + w + \frac{(80j+44k)}{3} \end{bmatrix}^{-1} \times \begin{bmatrix} 1 \\ 1 \\ 0 \end{bmatrix}. \quad (33)$$

Finally, in the case (iii), one of the two subcomponents of the central signal will be described by the equation

$$-Y_{C'}(\omega) = \begin{bmatrix} 1 & 1 & 0 & 0 \end{bmatrix} \times \begin{bmatrix} i\Delta\omega + w + \frac{80}{3}(j+k) & -\frac{16}{3}(j+k) & 0 & 0 \\ -\frac{16}{3}(j+k) & i\Delta\omega + w + 24j & \frac{8\sqrt{2}}{3}(j+k) & \frac{8\sqrt{2}}{3}(j+k) \\ 0 & \frac{8\sqrt{2}}{3}(j+k) & i(\Delta\omega + 3x) + w + \frac{(80j+44k)}{3} & -\frac{16}{3}(j+k) \\ & \frac{8\sqrt{2}}{3}(j+k) & -\frac{16}{3}(j+k) & i(\Delta\omega - 3x) + w + \frac{(80j+44k)}{3} \end{bmatrix}^{-1} \times \begin{bmatrix} 1 \\ 1 \\ 0 \\ 0 \end{bmatrix}, \quad (34a)$$

while the other will remain unaffected by the non-magnetic coherences, thus (c.f., Ref. [24])

$$-Y_{C''}(\omega) = (i\Delta\omega + w + 24j - 16k)^{-1} \quad (34b)$$

However, as was mentioned above, in the case of moderate quadrupolar relaxation (Eq. (31)) such a factorization is not possible and, therefore, the whole matrix **W** must be used for the description of the lineshape of A. The corresponding equation reads:

$$-Y(\omega) = F^T \mathbf{W}^{-1}(\omega) F \tag{35}$$

where

$$F^T = \begin{bmatrix} 1 & 1 & 1 & 1 & 1 & 1 & 1 & 1 & 1 & 0 & 0 \end{bmatrix}, \tag{36}$$

with the superscript T denoting a transpose of vector F.

When Eqs. (32)-(34b) are to be used in practical lineshape calculations, numerical problems may arise when the spectra are calculated using the standard approach of numerical diagonalization of the spectral matrix. This is because, especially for Eq. (34a) when the magnitude of J_{XX} is much smaller than $1/\pi T_{1Q}$, the matrices to be diagonalized are only in a trivial way different from real symmetric matrices. For matrices of such a form, the standard numerical routines designed to handle complex matrices usually calculate correct eigenvalues but incorrect eigenvectors. The numerical calculations leading to the curves in Fig. 2 were performed using a numerically stable method of matrix inversion [31]. A similar warning pertains to numerical calculations of the resolved spectra using the complete 11×11 matrix according to Eq. (35).

It should be noted that the relaxation-mediated couplings between the magnetic and non-magnetic coherences, entering Eqs. (32)-(35), would vanish only in a non-physical situation where the fluctuating quadrupolar interactions at the X nuclei were perfectly anti-correlated, in which instance the corresponding cross-correlation factor $r = k/j$ would be equal to -1. It should be also noted that for the perfect cross-correlation ($r = 1$) the non-magnetic coherences will attain a maximum strength in their influence on the bahaviour of the magnetic ones. The latter observation brings out the difference, exposed in detail in Ref. [25], between the notion of microscopic conservation of nuclear permutation symmetry [11] (which does apply to the system considered when $r = 1$) and that of conservation of magnetic equivalence symmetry. Note at the end that the coupling between the non-magnetic and the magnetic coherences do survive even when the nuclei X do not 'sense' each other directly, i.e. when both J_{XX} and r happen to vanish.

The situation to which Eqs. (34a)-(34b) are referred to is likely to be encountered in practice, especially for $^{13}CD_2$ spin groupings, since the corresponding deuterium-deuterium J-coupling constants are generally of the order of a fraction of a hertz and therefore fall in the range of deuterium quadrupolar relaxation rates in liquids of low and moderate viscosity. Experimental

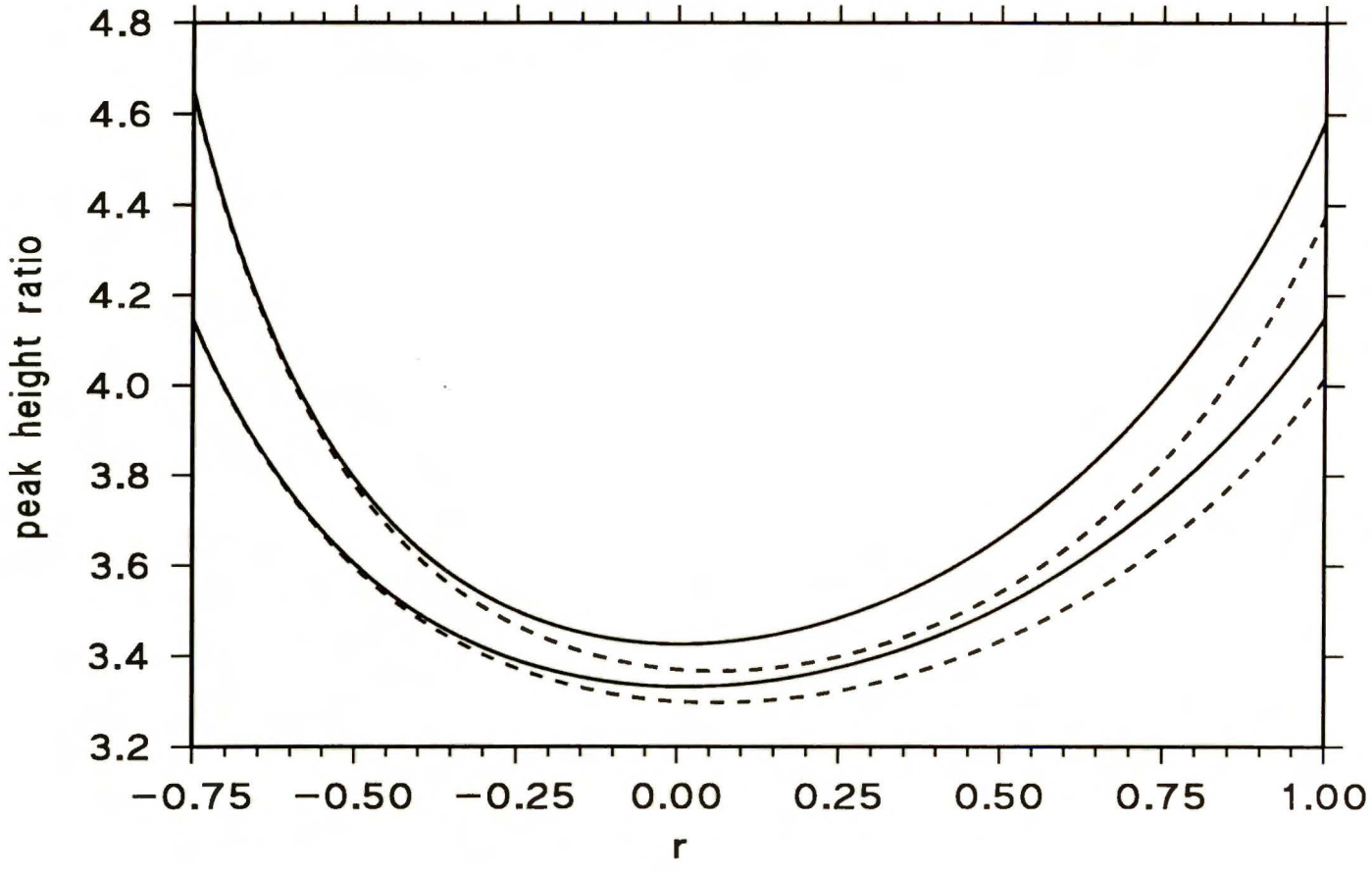

Figure 2: Theoretical dependences on quadrupolar cross-correlation factor of the height ratios of the central and outer components in the A pentet in AX_2 spin system, calculated with (solid lines) and without takin into account impact of the non-magnetic coherences on the lineshape. The calculations were performed for $J_{AX} = 21.5$ Hz, and the extraneous line broadening $w/\pi = 0.52$ Hz. The solid curves were calculated assuming $J_{XX} = 0.24$ Hz; for the top and bottom pairs of curves, the values of $j = (1/20T_{1Q})$ are 0.434 and 0.217 rad s^{-1}, respectively.

studies on quadrupolar cross-correlations in such a system in perdeuterated ethylene glycol are reported in the paper already cited Ref. [24]. The observed spectra were described in terms of the magnetic coherences only. Within such a simplified approach, the authors cited could in a unique way relate the ratios of heights of the central and inner peaks of the pentet to those of the outer peaks, h_c/h_o and h_i/h_o, respectively, to both the cross-correlation factor, r, an the 'extraneous' relaxation rate expressed in the units of j, $\rho = w/j$. The observed departures of the above lineshape parameters from their respective limiting 3:1 and 2:1 values (attainable in the limit of negligible quadrupolar relaxation) were proposed as quick measures of r in the instances where the magnitudes of ρ could be determined independently. Below I show that this generally usefull approach may be prone to substantial errors when applied to system with small or vanishing J_{XX} coupling constants. In Fig. 2 two pairs of h_c/h_o curves as a function of r are displayed. In the calculations, the values of J_{AX} (21.5 Hz) and w/π (0.52 Hz) were assumed according to the findings for deuterated ethylene glycol reported in Ref. [24]. In each pair, the solid curve was calculated according to Eqs. (34a)-(34b) in which the value of J_{XX} was put equal to 0.24 Hz, which is probably a maximum value for the geminal deuterium pair in ethylene glycol that could be expected [32]. The dashed curve is calculated from from Eq. (17) of Ref. [24], which gives the same results as our Eqs. (32) and (34a)-(34b) when a large value (but different from $2J_{AX}/3$) is substituted for J_{XX} in the latter equations. The bottom pair corresponds to the value of $j(T = 323K) = 0.217$ rad s^{-1} reported in Ref. [24]. The top pair was obtained assuming $j = 0.434$ rad s^{-1}. The display in Fig. 2 is limited to the values of r above -0.75. A consideration of the predictions based on the rotational diffusion model of molecular reorientations allows one to conclude that strongly negative values of r are unlikely to be encountered in practice. The corresponding pairs of h_i/h_o curves are not shown because in the case considered (the non-magnetic coherences interfering with the central component) our formalism would merely reproduce the results of Ref. [24].

Inspection of Fig. 2 reveals that for the system mentioned above the neglect of the non-magnetic coherences may impose a systematic bias on the assessment of r based on the lineshape parameter h_c/h_o. This is clearly seen if one compares the maximum difference between the corresponding values of h_c/h_o, calculated with and without taking into account the non-magnetic coherences, with the range of variations of this parameter in the displayed range of r. (Although the maximum difference generally occurs for r approaching 1, it is an adequate measure of the effect discussed since for r values above 0.5 both the curves go nearly parallel to each other.) For the top pair of curves, the maximum difference amounts to about 13 per cent of the whole variability

range, and it is increased to about 18 per cent when the parameter h_c/h_o is calculated assuming $J_{XX} = 0$. For the bottom pair, the corresponding figures are 12 and 20 per cent. The latter value is close to an upper limit of the discrepancies between the peak height ratios calculated in these two ways. For sake of transparency, the h_c/h_o curves calculated assuming $J_{XX} = 0$ are not shown in Fig. 2. Because even minor changes in the values of J_{XX} can lead to such significant variations of the course of the h_c/h_o curves, in order to get an unbiased estimate of r from the peak height ratio in resolved spectra, a very precise knowledge of the magnitude of J_{XX} may be required.

It can also be seen from the displayed curves that when the true value of J_{XX} is comparable with quadrupolar relaxation rate, the assessments based on the approximate theory will generally deliver overestimated values of $|r|$. A similar conclusion can be drawn regarding the use of the approximate lineshape equations in iterative analysis of the resolved spectra. Only in the instances where the true value of r falls below -0.3, the approximate approach becomes essentally equivalent to the exact approach, which was already anticipated from the form of the pertinent off-diagonal matrix elements in Eq. (34a).

3.1.2 Numerical simulations of spectral lineshapes.

One of the obvious conclusions of the preceding section is that, in different quadrupolar relaxation limits, the information content about quadrupolar cross-correlation, which is conveyed by the spectrum, may be different. As relaxation rates in liquids are sensitive to an average correlation time of the molecule, one can in some cases switch between different relaxation limits by changing experimental conditions such as temperature and solvent. Therefore, before starting NMR experiments it is worth-while to perform numerical simulations in order to learn which conditions should be choosen in order to obtain spectra carrying maximum information about the required parameters. I have carried out such simulations for a hypothetic spin system AX_2 using a computer program, similar to that mentioned earlier, written also by Szymański [27]. Selected results of these simulation are shown in Figs. 3-8 below. Columns 1-3 present theoretical dependence of standard spectra of spin A on the coupling constant between magnetically equivalent X nuclei, J_{XX}, in different quadrupolar relaxation limits, i.e. slow (0.628 rad s^{-1}, Column 1), moderate (1.885 rad s^{-1}, Column 2), and fast (3.770 rad s^{-1}, Column 3), compared to the coupling constant $J_{AX} = 10$ Hz. The values of J_{XX} are taken as 0.1 (solid lines), 5.0 (dashed lines) and 20.0 Hz (dotted lines). In the case of $J_{XX} = 0.1$ Hz the frequencies $\omega_{0A} \pm 3x$ of the non-magnetic coherences are very close to the center of the multiplet of A. When $J_{XX} = 5.0$ Hz, they are

still in the range of the multiplet frequencies, exactly in the middle between outer and inner of its components. For $J_{XX} = 20.0$ Hz the frequencies of the non-magnetic coherences are far away from the multiplet. For such values of J_{XX} the spectrum of A is almost independent of J_{XX}. One can easily see that the impact of these coherences on the signal shape reaches a maximum in the limit of moderate quadrupolar relaxation, whereas in the other limits it remains small or even negligible. Another inference from these simulations is that the signal distortions caused by the non-magnetic coherences seem to be stronger for high positive values of r.

Columns 4-6 present theoretical dependence of standard spectra of spin A on cross-correlation coefficient, r, in different quadrupolar relaxation regimes, for three values of J_{XX}: 0.1 Hz (Column 4), 5.0 Hz (Column 5), and 20.0 Hz (Column 6). In each picture, three curves are compared which correspond to high (95%, solid lines), low but still positive (30%, dashed lines), and negative (-50%, dotted lines) values of r. The dependence of the lineshapes on the coefficient r is observed for all assumed values of J_{XX} and j, but again in the limit of moderate quadrupolar relaxation it becomes the most significant.

The impact of both cross-correlation effects and J_{XX} on the spectra of A can be amplified by application of the Hahn-echo instead of the standard one-pulse pulse sequence. The Hahn-echo consists of a 90^0 pulse followed by delay τ, a 180^0 pulse, delay τ, and acquisition (see e.g. [33]). The spectrum of A obtained using this method is described by

$$Y_e(\omega) \sim F^T \mathbf{W}(\omega)^{-1} \exp[\mathbf{W}(\omega_0)\tau] \exp[\mathbf{W}'(\omega_0)\tau] F \tag{37}$$

where ω_0 is the spectrometer frequency and matrix $\mathbf{W}'$ differs from that $\mathbf{W}$ of Table (3.2) by substitution of $-\Delta\omega$ instead of $\Delta\omega$ and $-|J_{AX}|$ instead of $|J_{AX}|$. For longer delays τ, the overall signal amplitude of Hahn-echo is significantly decreased compared to the standard spectrum. This causes a loss of experimental sensitivity, but the desired effects are amplified due to different T_2 relaxation properties of the individual signal components. Simulated Hahn-echo spectra are displayed in Columns 7-12 of Figs. 6-8. The values of the parameters J_{AX}, J_{XX}, r, and j assumed in these simulations are exactly the same as those used in the calculations of the corresponding standard spectra in Figs. 3-5. The delay τ was assumed to be 50 ms for the spectra with $j = 0.628$ rad s^{-1}, and 20 ms for tha remaining spectra.

The presented simulations show clearly that quadrupolar cross-correlations significantly influence the spectral lines in both the standard and the corresponding Hahn-echo spectra of spin A, in a wide range of quadrupolar relaxation rates. The observed differences between the simulated spectra allow for a supposition that the cross-correlation spectral densities could under

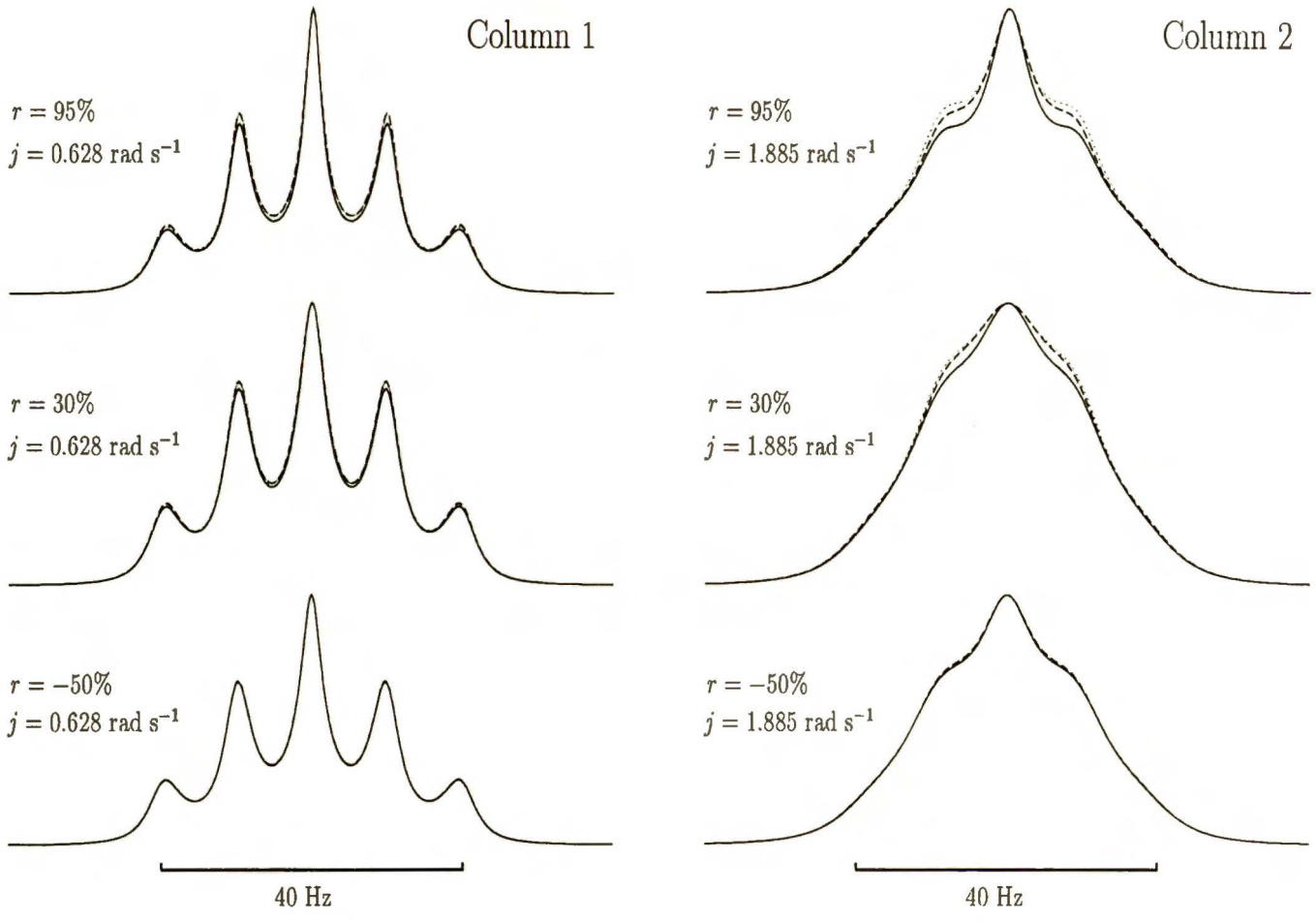

Figure 3: Dependencies of the standard spectra of A on the displayed values of j and r. The values of J_{AX} and of the field inhomogeneity broadening $w/2\pi$ are taken equal to 10 and 0.25 Hz, respectively. The superimposed spectra correspond to $J_{XX} = 0.1$ (solid line), 5.0 (dashed line) and 20.0 Hz (dotted line).

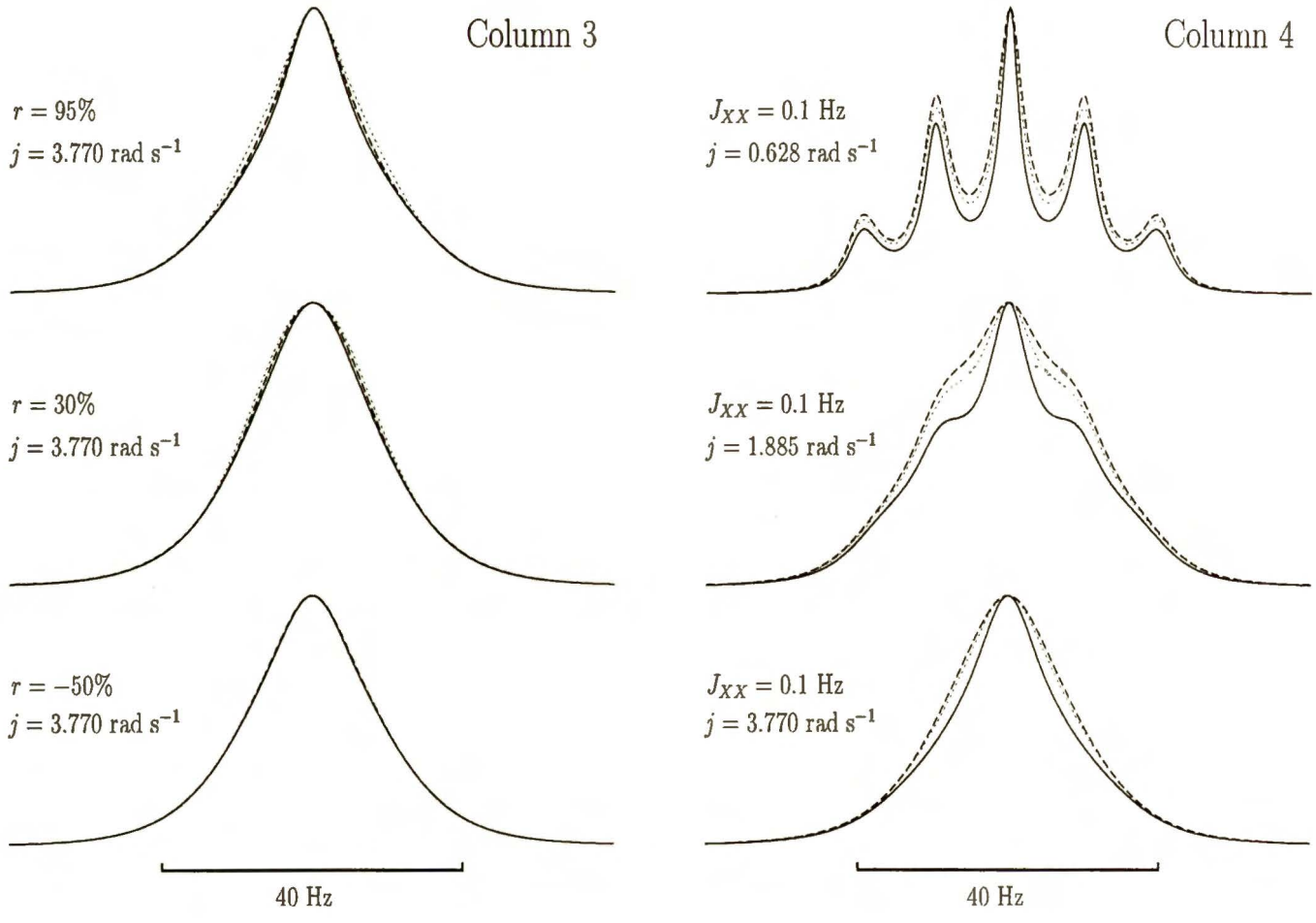

Figure 4: Column 3: Same as Fig. 3 but for $j = 3.77$ rad s^{-1}. Column 4: The superimposed spectra correspond to $r = -50$ (dotted line), +30 (dashed line) and +95% (solid line).

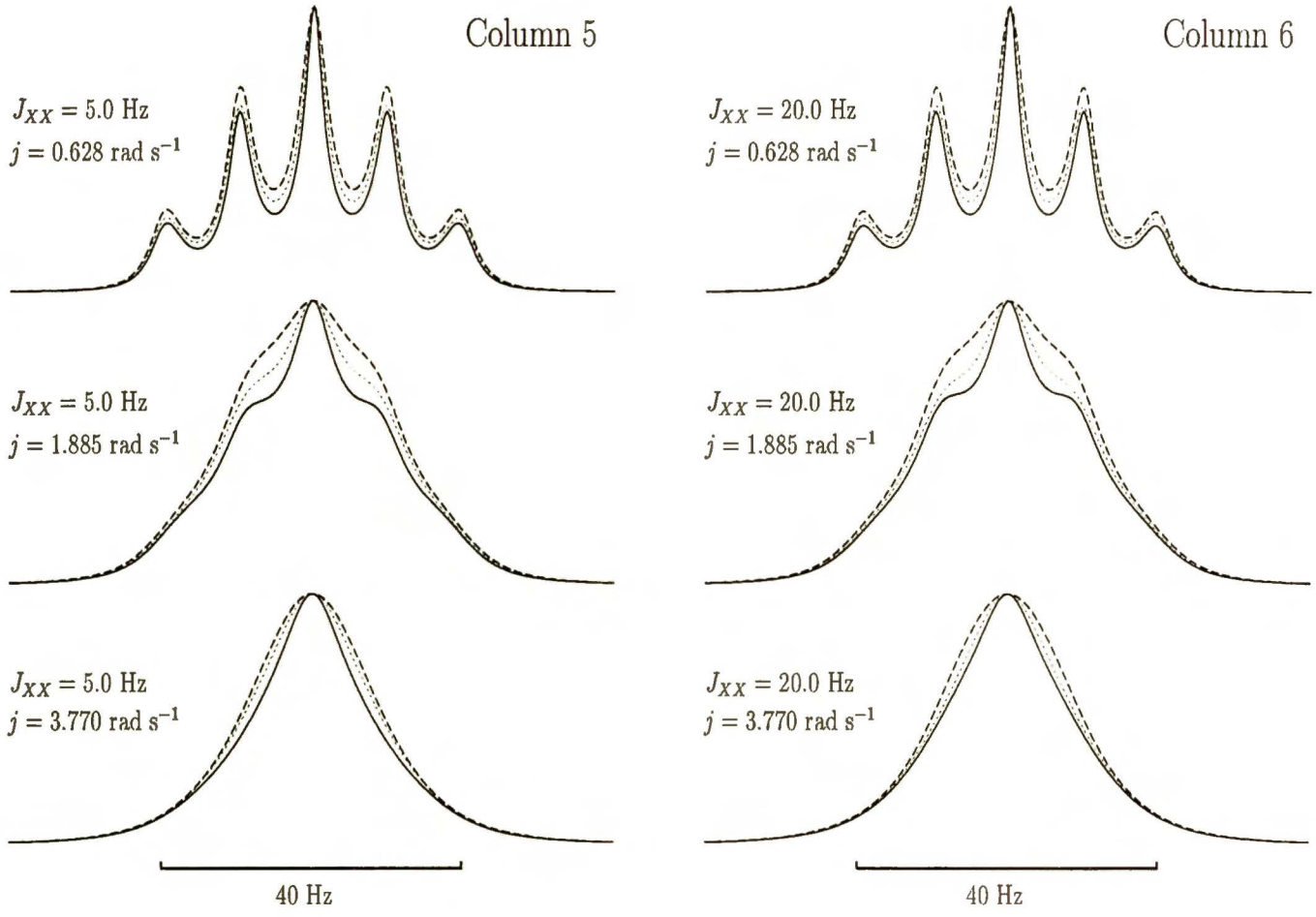

Figure 5: Same as Column 4 in Fig. 4 but for the values of $J_{XX} = 5$ and 20 Hz.

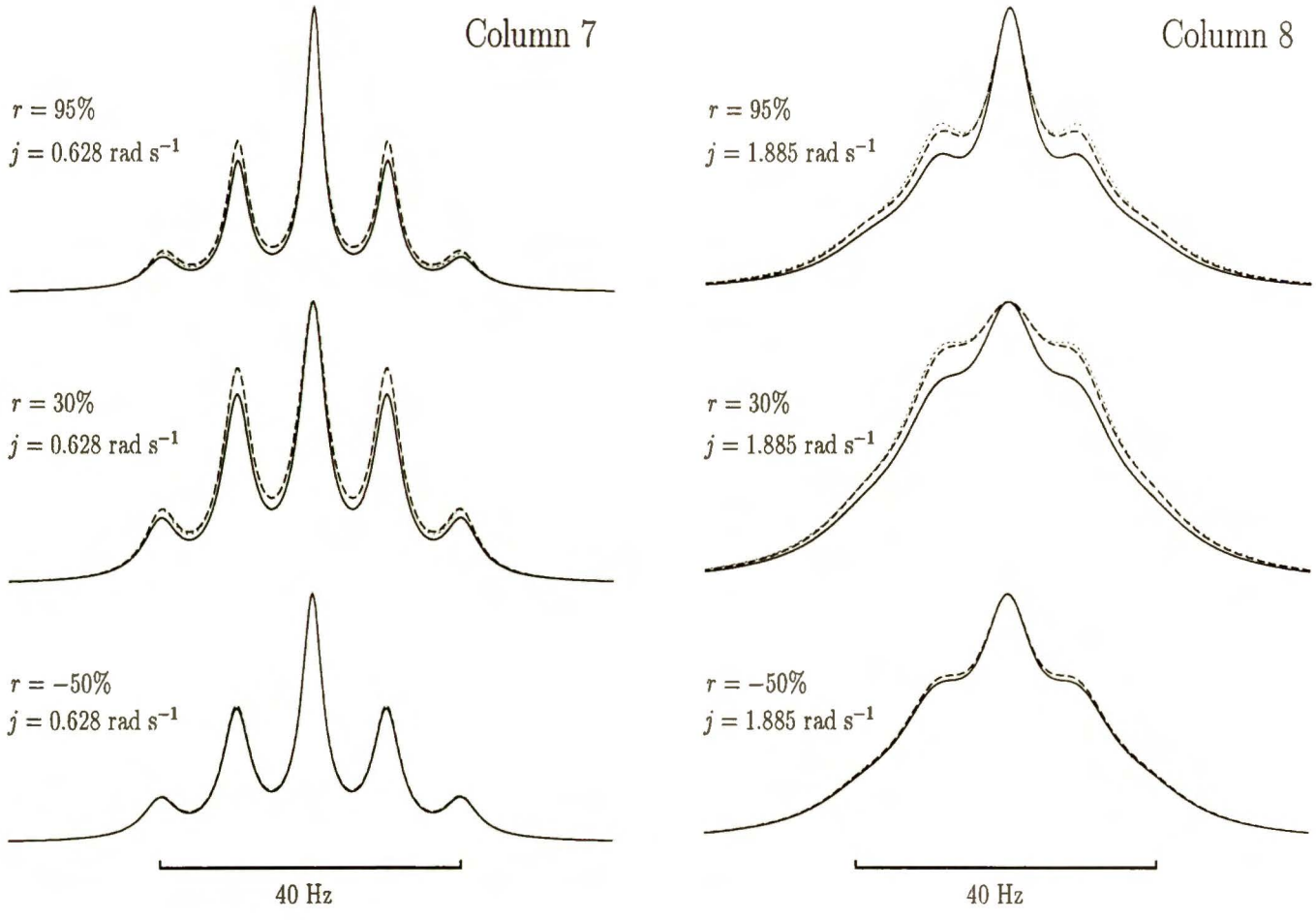

Figure 6: Same as Fig. 3 but for Hahn-echo spectra. Echo delay τ is 20 ms for $j = 1.885$ rad s^{-1} and 50 ms for $j = 0.628$ rad s^{-1}.

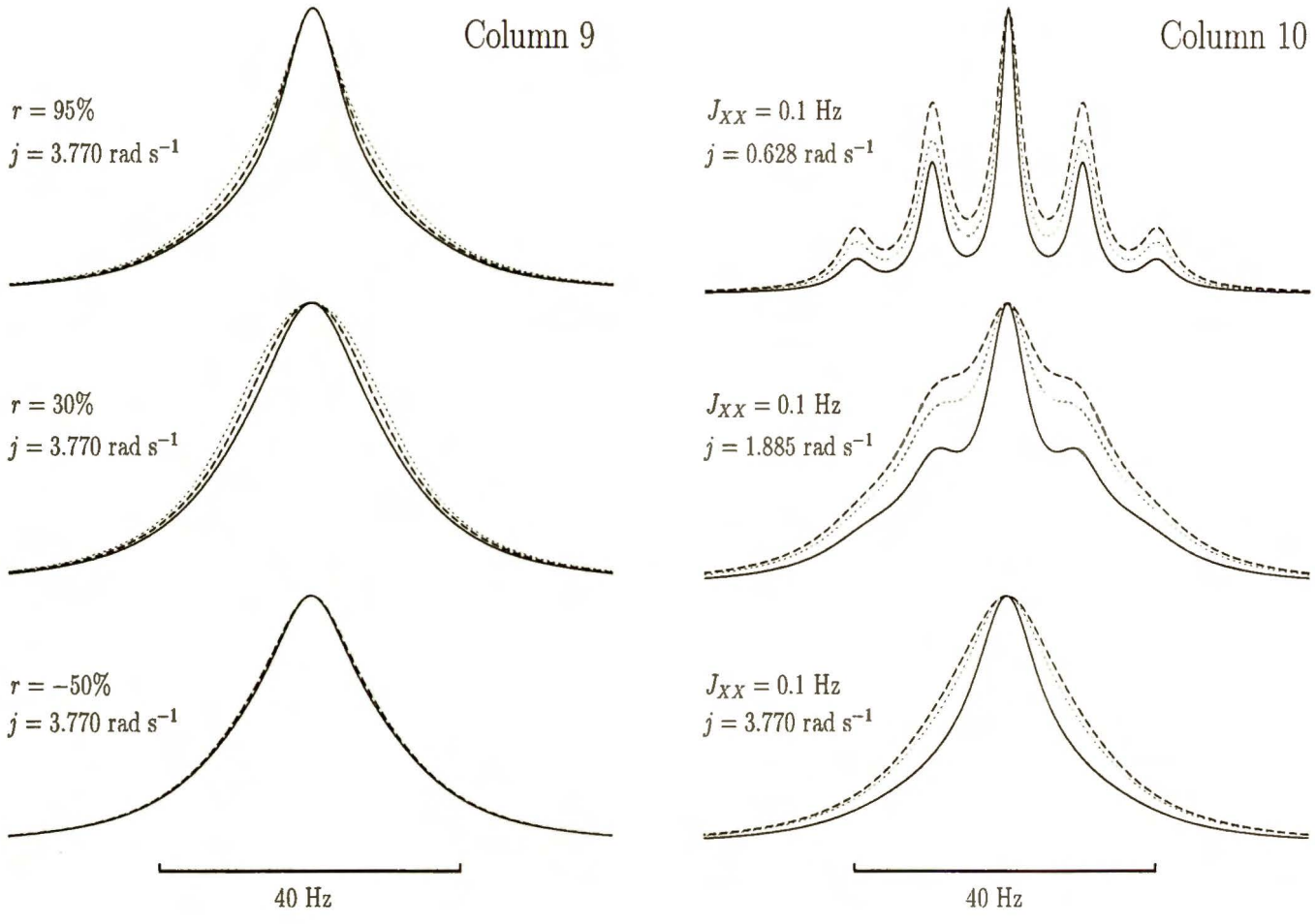

Figure 7: Same as Fig. 4 but for Hahn-echo spectra. Echo delay τ is 20 ms for $j = 1.885$ rad s^{-1} and 50 ms for $j = 0.628$ rad s^{-1}.

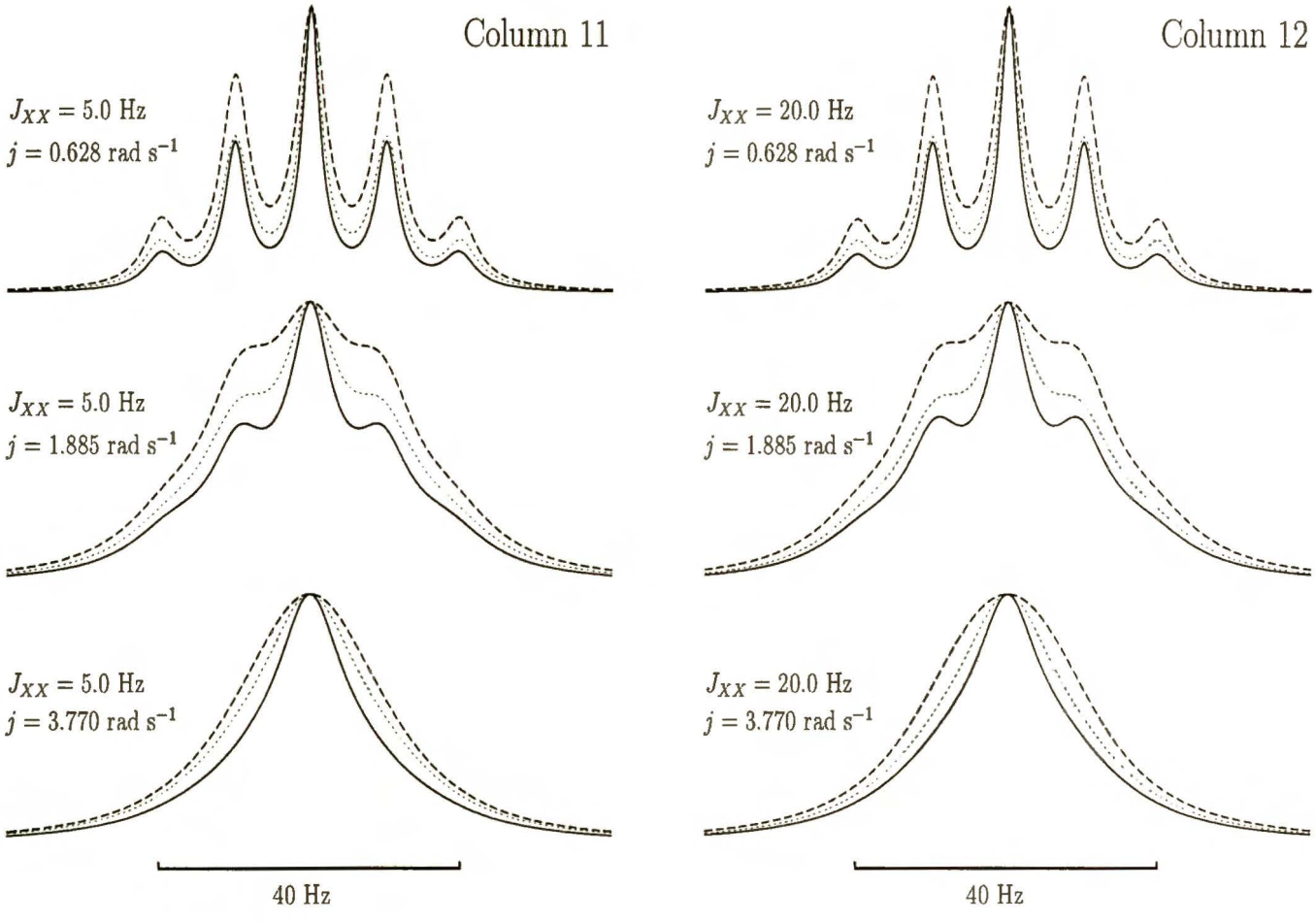

Figure 8: Same as Fig. 5 but for Hahn-echo spectra. The delay intervals τ assumed as in Figs. 6 and 7.

favourable conditions be quite easily determined from spectra by an iterative lineshape analysis. Also, the scalar coupling, J_{XX}, between magnetically equivalent quadrupolar nuclei, seems to be derivable from the spectrum of A measured in moderate quadrupolar relaxation limit.

3.2 Practical evaluation of nuclear quadrupolar cross-correlations.

In this chapter I use two molecular models, i.e. 2,1,3-benzoselenadiazole and azide anion ^{14}N-^{15}N-^{14}N, to demonstrate problems concerned with practical application of the algorithms of quadrupolar cross-correlations evaluation. Careful analysis of the problems resulting from both low absolute value of cross-correlation and lack of knowledge of the value of scalar coupling between magnetically equivalent nuclei, allows for an elaboration of the methodology involved. This is a necessary prerequisite for further application of cross-correlations in the investigations of molecular structure and dynamics.

3.2.1 Low cross-correlation. Analysis of ^{77}Se and ^{14}N spectra of 2,1,3-benzoselenadiazole.

One-bond scalar spin-spin couplings of ^{77}Se (spin-1/2) to nitrogen are usually large and can be comparable with quadrupolar relaxation rates of ^{14}N nuclei in non-viscous liquids [34, 35]. At room temperature, the ^{77}Se signal in a benzene solution of the 2,1,3-benzoselenadiazole **1** is substantially broadened; its width-at-half height is equal to 120 Hz while the width of the ^{14}N signal is about 240 Hz. The characteristics of the relevant electric field gradient (EFG) tensors, calculated at a DFT level [36], are given in Fig. 9. The molecular geometry assumed in the calculations of the EFG's was optimized using TURBOMOLE program with the DFT option [37]. I previously managed to determine the ^{77}Se-^{15}N coupling constant of 105 ± 0.2 Hz (for 0.5 mol/liter solution of **1** in DMSO at 320 K) from the ^{77}Se satellites (natural abundance 7.58%) in the natural-abundance ^{15}N spectrum [35]. Using the relationship

$$\Delta W = (8/3) J^2 \pi T_{1Q} \tag{38}$$

(see e.g. Ref. [2]), where ΔW is the broadening of ^{15}N signal and T_{1Q} is the longitudinal relaxation time of the ^{14}N nucleus, I could also assess the absolute magnitude of the ^{15}N-^{14}N coupling constant to be smaller than 7.5 Hz.

Under the conditions of proton decoupling, the ^{77}Se nucleus coupled to two ^{14}N nuclei can be together considered as AX_2 spin system. Therefore, the ^{77}Se spectra of **1** can be described by matrix **W** (c.f. Table 3.2) and Eq. (35). For

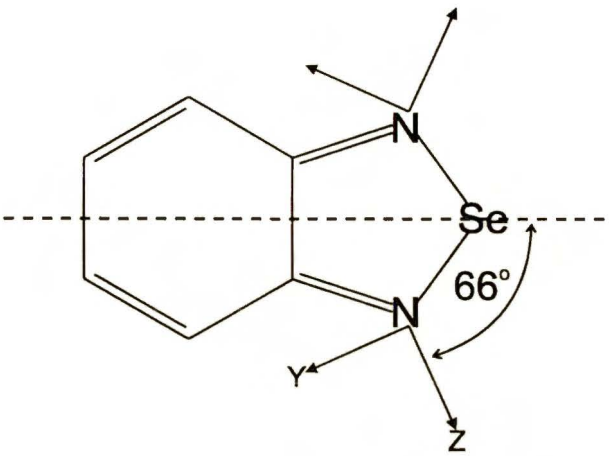

Figure 9: Principal axes of the EFG tensor, calculated at a DFT level, for the nitrogen nuclei in 2,1,3-benzoselenadiazole, **1**. The principal values (MHz) are $V_{zz} = -3.68$, $V_{yy} = 2.40$, and $V_{xx} = 1.28$ ($\eta = 0.304$).

the analysis of the spectra, or, optionally, the FID functions, of both the ^{77}Se and ^{14}N subsystems simultaneously, I used the above-mentioned iterative computer program [27]. In the description of the ^{14}N signals of **1**, the contributions of both the isotopomers of **1**, containing magnetically active and non-active selenium isotopes, were accounted for. At ambient and elevated temperatures, the proton-decoupled ^{77}Se spectra of **1** can in principle be sensitive to each of the NMR parameters entering matrix **W**. The proton-decoupled ^{14}N spectra, on the other hand, are sensitive only to J_{AX} and j in the whole temperature range where the extreme narrowing approximation is applicable [25]. Convergence problems in the simultaneous iterative analysis of the ^{77}Se and ^{14}N spectra ought therefore to be much less severe than in the case of separate analyses. Actually, in the numerical computations described below no such problems have occured despite the fact that at each temperature up to 12 lineshape parameters were varied simultaneously. Eight of them: amplitudes, baseline levels, dispersion admixtures, and positions of the resonances at the respective frequency axes are of no interest in the present context but they are critical for the quality of the fits.

Keeping in mind the results of my earlier simulations, I performed iterative analysis of the pairs of spectra of **1** measured at four different temperatures. The unknown a priori value of J_{XX} was kept fixed. At each temperature, the calculations were performed for three values: 0, 5 and 40 Hz, of J_{XX}. For both ^{77}Se and ^{14}N spectra, the magnitude of $1/\pi T_2^*$ was set to 0.2 Hz, which

seemed reasonable since the line widths in the ^{1}H spectra measured for the same sample using the same NMR probe never exceeded 1 Hz (the contribution to the ^{77}Se linewidth of the ^{77}Se T_2-processes I assess to be negligible). For the runs with the assumed values 0 and 5 Hz of J_{XX}, the results delivered by the fitting algorithm at convergence were practicaly the same, regardless of whether the FID functions (including the data from both channels of the receiver) or the corresponding absorption spectra were taken as the input data. However, such an agreement could be achieved only when (i) at any stage of the fitting process the spectra calculated according to Eq. (35) were numerically broadened by convolution with the corresponding sinc function, $\sin(2\pi\nu t_{max})/\nu t_{max}$, where t_{max} is the acquisition time, and (ii) in the analysis of the FID's, the first 4 or 8 points of the experimental FID functions were rejected (see caption to Fig. 11). Results of the lineshape analysis are collected in Table 3.3. The experimental ^{77}Se and ^{14}N spectra with the superimposed "best fit" theoretical spectra are displayed in Fig. 10, and for the experiment at 393 K, the corresponding ^{77}Se FID functions are shown in Fig. 11. In a related context, it was found advantageous to use in the lineshape analysis the FID's instead of the spectra [38]. This opinion is not supported by the

Table 3.3: Results of lineshape analysis of the ^{77}Se and ^{14}N spectra of **1**. Numbers without and within parentheses were obtained under assumption of $|J_{XX}| \leq 5$ Hz and $|J_{XX}| = 40$ Hz, respectively; standard errors are given.

T(K)	J_{AX}(Hz)	$j(rad\,s^{-1})$	$k(rad\,s^{-1})$	$r = k/j$
303[a]	78.0 ± 0.3	124.5 ± 0.5	37.4 ± 22.0	0.30 ± 0.18
	(78.3 ± 0.3)	(125.2 ± 0.4)	(67.2 ± 7.0)	(0.54 ± 0.06)
343[a]	76.7 ± 0.3	73.4 ± 0.3	11.0 ± 8.6	0.15 ± 0.12
	(77.2 ± 0.3)	(73.2 ± 0.3)	(39.2 ± 2.4)	(0.54 ± 0.03)
383[a]	76.6 ± 0.2	50.6 ± 0.2	1.0 ± 40.4	0.0 ± 0.8
	(76.9 ± 0.2)	(50.6 ± 0.2)	(25.2 ± 1.4)	(0.50 ± 0.03)
393[b]	76.3 ± 0.2	53.4 ± 0.3	5.1 ± 11.1	0.10 ± 0.21
	(76.7 ± 0.2)	(53.6 ± 0.2)	(27.8 ± 0.9)	(0.52 ± 0.02)

[a] Benzene solution.

[b] Toluene solution.

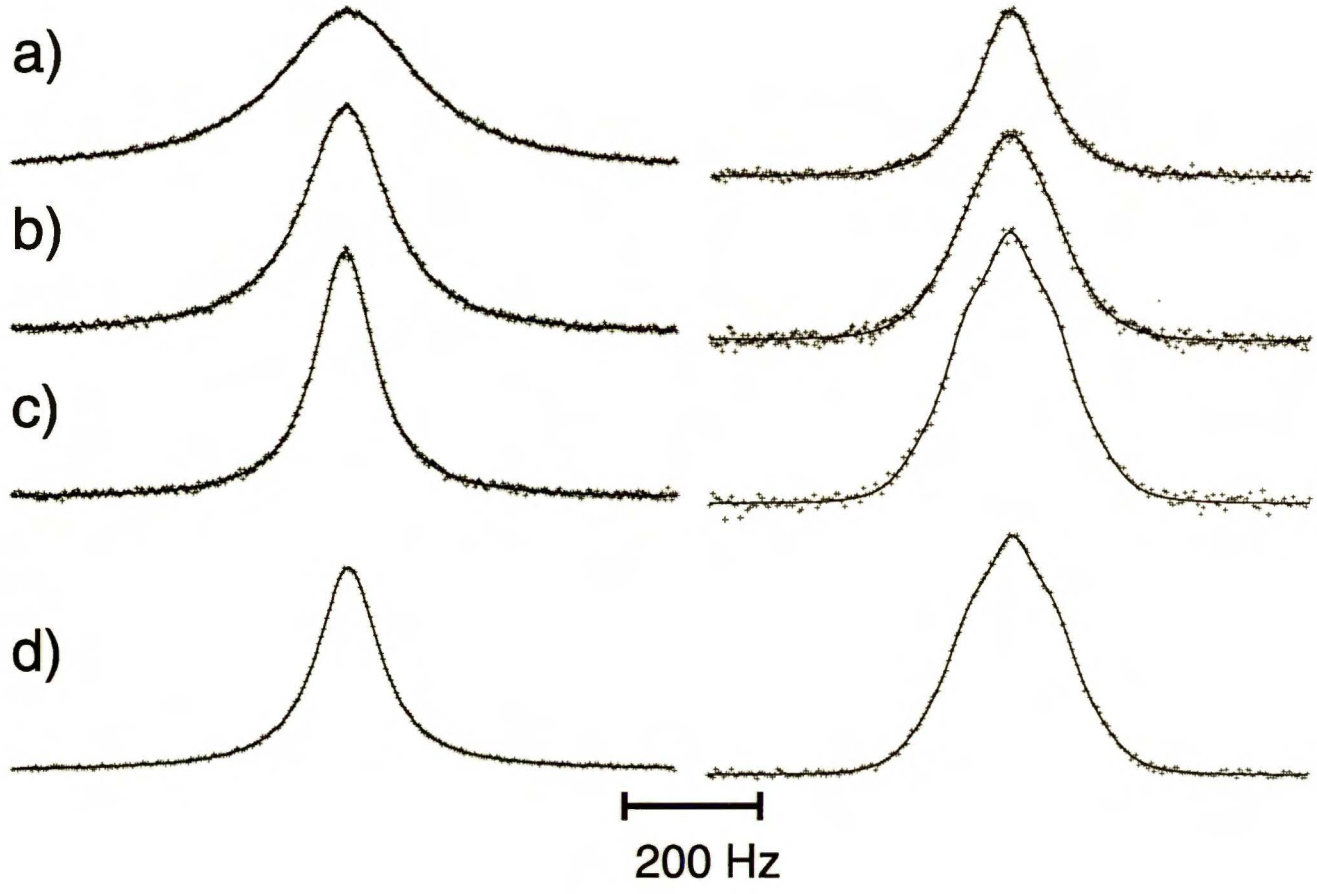

Figure 10: Experimental $^{14}N\{^1H\}$ (left side) and $^{77}Se\{^1H\}$ (right side) spectra, measured at 303 (a), 343 (b), and 373 K (c) for a benzene solution of **1** and at 383 K for a toluene solution of **1** (d). The solid curves depict the superimposed "best fit" theoretical spectra.

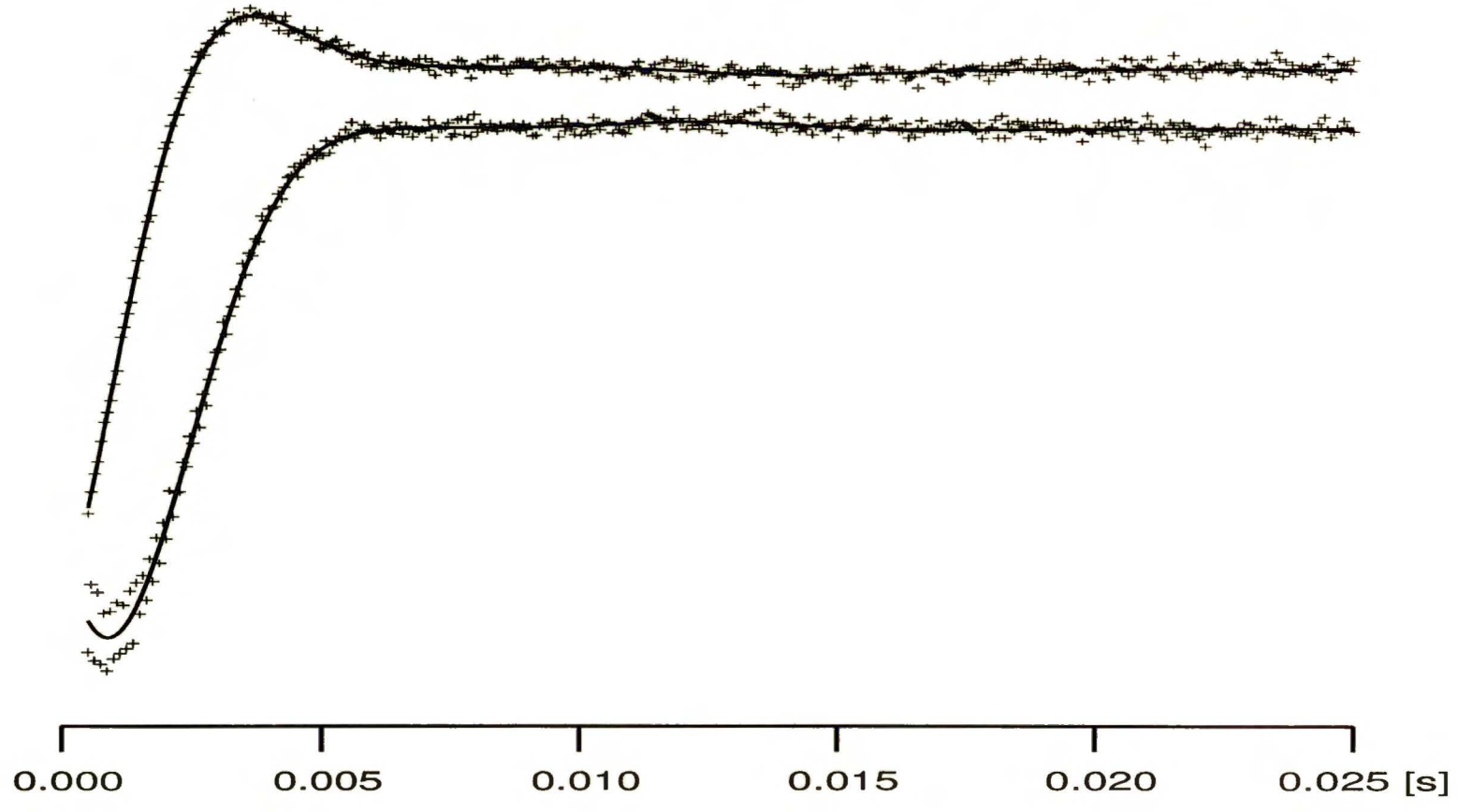

Figure 11: Experimental (crosses) and theoretical "best fit" (solid lines) FID functions of the $^{77}Se\{^{1}H\}$ resonance in toluene solution of **1** at 393 K. The displayed components of the experimental FID were obtained from the raw data, registered in a digital mode, using CONVDTA program provided by the Bruker company. The first 4 points of the preprocessed data were rejected. The remaining 12 initial points from one of the receiver channels (lower plot) are still distorted, which is probably due to an incomplete removal, by the CONVDTA program of the digital filter characteristics contained in the raw data. Retention of these 12 points in the input data for the least-squares calculations does not significantly affect the results.

results reported presently. As can be seen from the data in Table 3.3, the results for J_{AX}, and j are essentially independent on the assumed value of J_{XX}. The estimated J_{AX} does not differ much from the value of 75.5 Hz calculated from the value of ^{77}Se-^{15}N coupling constant measured directly [35]. The most accurate are preasumably the estimates of J_{AX} extracted from the spectra at 383 and 393 K, in which outlines of the fine structure start to emerge. For the reasons to be clarified later on, as the most reliable I consider the results obtained under assumption of $|J_{XX}| \leq 5$ Hz. Therefore, I take the value of 76.5 ± 0.2 Hz as the result for the ^{77}Se-^{14}N coupling constant; the discrepancy of 1 Hz relative to the value derived from ^{77}Se-^{15}N coupling constant may be due to a primary ^{14}N/^{15}N isotope effect. The values of k obtained under the assumption of $|J_{XX}| \leq 5$ Hz point to a low degree of quadrupolar cross-correlations in the systems considered (benzene and toluene solutions of **1**) in the whole temperature range. These values come with large standard errors, which is not surprising in the case of the spectra measured at 303 and 343 K, because such are the expectations from the spectral simulations mentioned earlier. However, the large standard error of k at 383 K is in a striking contrast to the expectations. I first blamed for this the relatively low signal-to-noise ratio in the ^{77}Se spectrum at 383 K. The high-temperature experiment was therefore repeated for a toluene solution of **1** in which experiment a significant improvement of the quality of the spectrum was achieved. This however did not reduce the magnitude of the standard error of k at a satisfactory level. Then I found out that for small values of $|r|$ the lineshape functions calculated for k and $-k$ are practically non-differentiable. Accordingly, for the values of $|r|$ approaching 0 the two equivalent minima at the sum-of-squares hypersurface, those at k and $-k$, may merge into a single, broad minimum, the exact position of which may strongly react to even a slight perturbation by the random noise. In the limit of slow quadrupolar relaxation, similar conclusion as to the limited sensitivity of the signal shape to the values of r varying around zero can also be drawn from inspection on the curves in Fig. 2. Thus, the results obtained for k can only be interpreted semiquantitatively. Nevertheless, the conclusion that in the high temperature limit the quadrupolar cross-correlations are very low for the benzene and toluene solutions of **1** seems fully justified. It is interesting to note that for the calculated electric field gradient tensors (see caption to Fig. 9) and under assumption of an anisotropic rotational diffusion, described by the ratio of the diffusion coefficients $D_Z : D_Y : D_X = 5.33 : 1.00 : 1.23^{\dagger}$, the theoretical value of r calculated according to Eq. (24) amounts to -0.111.

[†]Following Ref. [39], these three values are taken to be proportional to the reciprocals of the corresponding principal values of the moment of inertia tensor of **1**.Axis Z is the symmetry axis of the molecule and axis Y is perpendicular to the plane of the molecule

This is in a fair correspondence with our estimate. As far as I know, this is the first successful attempt to determine quadrupolar cross-correlations in isotropic fluids.

The results for k obtained under assumption of J_{XX}=40 Hz differ significantly from zero (note their small standard errors), which is a clear confirmation of the fact already predicted theoretically [25] that in the spectrum of spin-1/2 nucleus scalar coupled to two equivalent quadrupolar nuclei the estimates of J_{XX} and r will show up substantial statistical correlation. In the present case, the results obtained under assumption of $|J_{XX}| > 5$ Hz can be rejected on the basis of the already mentioned data obtained for the DMSO solution of **1**. The observed statistical correlation provides an indirect proof of the spectroscopic relevance of J-couplings between magnetically equivalent quadrupolar nuclei. Studies on a related system in which $|r|$ is close to unity provide a more direct evidence of this property. Such studies are described in the next chapter.

Experimental. Compound **1** was synthesized by Bjørlo and Mørkved from the University of Trondheim according to a published procedure [40]. Proton-decoupled NMR spectra of ^{77}Se and ^{14}N in **1** were measured using Bruker Avance DRX 500 MHz spectrometer, equipped with a BVT 3000 temperature unit and a broadband probe, in the temperature range of 303-393 K. The samples containing c.a. 0.2 mol/liter and 0.3 mol/liter solutions of **1** in benzene-d6 and toluene-d8, respectively, were degassed and sealed under vacuum of about 0.1 torr in NMR tubes (WILMAD, o.d. 5mm, i.d. 3.44mm). The ^{77}Se spectra were recorded by applying a 20-degree pulse with repetition time between 117 and 225 ms, depending on the signal width. Up to 350,000 scans (11 hours) were recorded. Possible distortions of the ^{77}Se lineshapes due to incomplete recovery of the system between the pulses seem negligible; no interference T_1-relaxation mechanisms that might cause a multiexponential recovery can be identified for the ^{77}Se nucleus in **1**.

At high temperatures, problems with unexpected, uncontrolled and very rapid solvent boiling occured, which could lead to a peril of sample damage inside the spectrometer magnet. This effect was probably a result of temperature gradient in the sample which is small at room and slightly elevated temperatures, but is significantly increased at 363-393 K. My further experience, gained in the measurements on the azide anion described below, is that such an effect can be avoided by using samples sealed without degassing.

3.2.2 The significance of J-coupling between magnetically equivalent nuclei. Analysis of NMR spectra of the azide ^{14}N-^{15}N-^{14}N anion.

From an earlier study it follows that azide ion N_3^- of sodium azide NaN_3 can be assumed to have at least a C_{2v} symmetry on NMR time scale [41]. If this anion was linear (symmetry $D_{\infty h}$) on the time scale of molecular tumbling, then one could expect rather high value of quadrupolar cross-correlations between the two terminal, magnetically equivalent ^{14}N nuclei. For high values of r, from the lineshape simulations described in Section 3.1.2, a substantial dependence of spectra of the central nitrogen atom on r and $^2J_{XX}$ can be expected. Comercially available sodium azide consists of three ^{14}N atoms. Lineshape simulations performed by me have proved that the effects in question can in principle be observed in spectra of such a molecule. However, due to a small value of the couplings $^1J(^{14}N\text{-}^{14}N)$ between the central and terminal nuclei and relatively fast quadrupolar relaxation causing undesired line broadening of the central ^{14}N nucleus, they may be not large enough to allow for an accurate evaluation of the required parameters. In order to have these effects amplified, I have synthesized sodium azide **2** 95% ^{15}N-selectively labelled in the central position. In the labelled compound, the value of one-bond coupling constant between the central and terminal nitrogen nuclei is increased by a factor of 1.4 (the magnetogyric ratio of ^{15}N is 1.4 times greater than that of ^{14}N), and the line broadening of the central nucleus is greatly reduced(^{15}N is a spin-1/2 nucleus). For **2** dissolved in D_2O, upon increasing the temperature up to 383 K, I have managed to reach the regime in which the $^1J(^{15}N\text{-}^{14}N)$ = 11.59 Hz[†] was of the same order of magnitude as the quadrupolar relaxation rate of the terminal ^{14}N nuclei. At this temperature, and also at 353 K, I have measured standard spectra of the ^{15}N and ^{14}N nuclei; for the latter nucleus, also T_1-relaxation time at 383 K was determined. Unfortunately, despite of very long acquisition runs, lasting almost 70 hours at each temperature, the signal-to-noise ratio in ^{15}N spectra was rather poor (see Fig. 12). The main reason of this problem was extremely long T_1 relaxation time of the ^{15}N nucleus, extrapolated from the T_1 values obtained at lower temperatures, to be about 60 seconds at 383 K and about 65 seconds at 353 K (the unexpected increase of relaxation rate at the higher termperature is probably caused by spin-rotation relaxation mechanism, which seems to by quite important for the discussed molecule). The painful but unavoidable consequence of the poor quality of the ^{15}N spectra was low accuracy of the fits,

[†]This value, determined by me at T=353 K, favourably compares with that of 11.32 Hz obtained in Ref. [42] for ^{15}N-^{15}N-^{15}N azide.

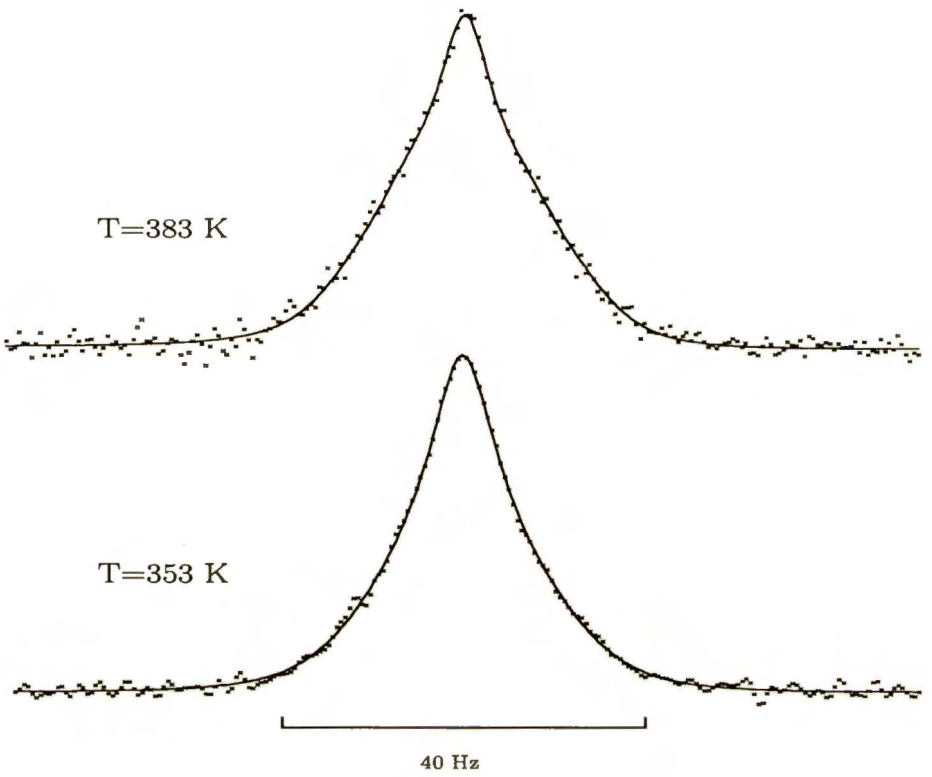

Figure 12: Experimental ^{15}N spectra of azide ion selectively ^{15}N-labelled in central position **2** superimposed with the "best fit" calculated spectra. The fits displayed were obtained under assumption of $^2J_{XX} = 0.1$ Hz (see text).

what was disappointing from the point of view of my main goal. Namely, my primary aim was a simultaneous determination of both $^2J_{XX}$ and r. Despite of the use of different fitting strategies (see below), I was not successful. The value of $^2J_{XX} = 4.3 \pm 1.5$ Hz delivered by the fitting program at convergence, was accompanied by the estimate of r exceeding 100%, which is non-physical. I can only estimate that in order to quantitatively measure the value of $^2J_{XX}$ from the spectra of the central nitrogen nucleus, I would have to perform the signal acquisition for at least 200 hours. Such experiments were not possible because of technical reasons. Therefore, I decided to focus my effort on the possibly most exact determination of coefficient r, whose overall impact on the spectra is stronger than that of $^2J_{XX}$. The quality of ^{15}N spectra has finally appeared to be good enough for such a purpose. From line broadening

Table 3.4: Results of lineshape analysis of the ^{15}N and ^{14}N spectra of **2**. Numbers without parentheses, within curly brackets and within parentheses were obtained under assumption of $|J_{XX}| = 0.1$, 5.0, and 10.0 Hz, respectively; standard errors are given.

$w(^{14}N)/2\pi$	$w(^{15}N)/2\pi$	$j(rad\,s^{-1})$	$k(rad\,s^{-1})$	$r = k/j$
		T=383K		
0.79 ± 0.20	0.41 ± 0.13	2.36 ± 0.06	2.27 ± 0.10	0.962 ± 0.04
$\{0.60 \pm 0.21\}$	$\{0.57 \pm 0.14\}$	$\{2.41 \pm 0.06\}$	$\{2.60 \pm 0.10\}$	$\{1.079 \pm 0.04\}$
(0.06 ± 0.24)	(0.82 ± 0.15)	(2.58 ± 0.07)	(2.92 ± 0.11)	(1.132 ± 0.04)
		T=353K		
1.26 ± 0.23	0.41 ± 0.12	3.22 ± 0.07	3.07 ± 0.11	0.953 ± 0.03
$\{1.07 \pm 0.26\}$	$\{0.48 \pm 0.13\}$	$\{3.28 \pm 0.08\}$	$\{3.34 \pm 0.11\}$	$\{1.018 \pm 0.03\}$
(0.12 ± 0.32)	(0.60 ± 0.14)	(3.58 ± 0.10)	(3.77 ± 0.13)	(1.050 ± 0.04)

of the signals of the terminal ^{15}N nucleus in the azide ion labelled with ^{15}N in central and one of the terminal positions, which I also synthesized, using the relationship in Eq. (38), I managed to determine the upper limit for the value of the critical parameter $^2J_{XX}$ to be 0.1 Hz.

For each of the mentioned temperatures, both the ^{15}N and ^{14}N spectra of **2** were analysed simultaneously, similarly as was done for **1**. The fits were performed for three fixed values of $^2J_{XX}$, 0.1, 5.0 and 10.0 Hz. Calculations for the values of $^2J_{XX} = 5.0$ and 10.0 Hz were performed for sake of a comparison. Results of these iterative analyses are given in Table 3.4. For the realistic value of $^2J_{XX} = 0.1$ Hz the cross-correlation coefficient r determined from the analysis is very close to unity, but still falls below it. When $^2J_{XX}$ is increased to 5.0 Hz, for both temperatures the obtained values of r exceed 100% and become thus non-physical. For $^2J_{XX} = 10.0$ Hz, the "best fit" value of r at $T = 383$ K exceeds 100% by more than three standard errors. Despite of the fact that it was obtained in an indirect way, this seems to be the first unquestionable experimental evidence of the dependence of the spectra on the scalar coupling constant between magnetically equivalent nuclei.

In the left-hand column of Table 3.4 one can follow variations of the "best fit" values of $w(^{14}N)$. They seem to be overestimated in the case of small $^2J_{XX}$, but are significantly decreased in the remaining cases. To eliminate the possible impact of this artificial degree of freedom on the estimates of r, for the experiment at 383 K I decided to apply another fitting strategy in which

Table 3.5: Refined results of lineshape analysis of the ^{15}N spectra of **2**. Numbers without parentheses, within curly brackets, and within parentheses were obtained under assumption of $|J_{XX}| = 0.1$, 5.0, and 10.0 Hz, respectively; standard errors are given. Spectral density j calculated from ^{14}N T_1 relaxation times was 2.375 rad s^{-1} for temperature 383 K. The value of $j = 3.399$ rad s^{-1} was used for temperature 353 K (see text for explanation).

$w(^{15}N)/2\pi$(Hz)	$k(rad\,s^{-1})$	$r = k/j$
	T=383K	
0.45 ± 0.14	2.30 ± 0.08	0.968 ± 0.034
$\{0.50 \pm 0.14\}$	$\{2.54 \pm 0.06\}$	$\{1.069 \pm 0.025\}$
(0.50 ± 0.14)	(2.62 ± 0.06)	(1.103 ± 0.025)
	T=353K	
0.66 ± 0.08	3.33 ± 0.07	0.980 ± 0.021
$\{0.65 \pm 0.07\}$	$\{3.49 \pm 0.05\}$	$\{1.027 \pm 0.015\}$
(0.56 ± 0.08)	(3.55 ± 0.04)	(1.044 ± 0.012)

the value of j was derived from T_1 relaxation time of the ^{14}N nuclei instead of extracting it from the ^{14}N spectrum. At 353 K, $T_1(^{14}\text{N})$ relaxation time was unfortunately not measured. In order to obtain an estimate of j at 353 K unbiased by the lack of knowledge of $w(^{14}\text{N})$, I fitted "extraneous" line broadening of the ^{14}N line at temperature 383 K under assumption of fixed spectral density j taken from the ^{14}N T_1 measurement in this temperature. Then this value of $w(^{14}\text{N})$ was used for fitting of the spectral density j from the ^{14}N spectrum measured at 353 K. The result of this procedure, $j = 3.399$ rad s^{-1}, was used in further iterative analysis of spectra of ^{15}N at 353 K. The fitted ^{15}N spectra for both temperatures are shown in Fig. 12. Numerical results of the modified fitting procedure are reported in Table 3.5. In contrast to the results of the previous fitting strategy, these refined estimates of the "extraneous" line broadening $w(^{15}N)/2\pi$ seem to be essentially identical for all six fits. This is reasonable if one takes into account that both the ^{15}N spectra were recorded in the same magnet using the same probehead. Therefore, stability of the value of $w(^{15}N)$ can be probably treated as a good test of reliability of the above results. It is worth to note that for large (compared to w) values of j and $^1J_{AX}$ in an investigated system, the discussed uncertainty of the value of w is immaterial.

In view of the results of the modified strategy, the main conclusions derived from analysis of the data in Table 3.4 remain still valid, i.e. correlation coefficient r is very high (at least 96.8%) in the investigated case, and the ^{15}N spectrum of the central nitrogen atom is dependent on the coupling constant between magnetically equivalent nuclei, $^2J_{XX}$. The high value of r confirms that in the solution studied, the azide anion retains $D_{\infty h}$ symmetry not only on the NMR time scale but also on the timescale of molecular tumbling.

Experimental. Both sodium azides, ^{14}N-^{15}N-^{14}NNa **2** and ^{14}N-^{15}N-^{15}NNa, were synthesized by me according to a published procedure [43]. NMR spectra of ^{14}N and ^{15}N in **2** were measured using Bruker Avance DRX spectrometer, equipped with a BVT 3000 temperature unit and a broadband probe, at two temperatures of 353 and 383 K. The sample containing c.a. 100 mg of sodium azide **2** and 100 mg of sodium carbonate in 1.5 ml of D_2O was sealed under ambient pressure in NMR tubes (WILMAD, o.d. 10mm, i.d. 7.12mm). The ^{15}N spectra were recorded by applying 90-degree pulse with repetition time 350 s. (longer than fivefolded T_1 relaxation time of the pulsed nucleus). Up to 705 scans (69 hours) were recorded. The ^{14}N spectra were recorded by applying 90-degree pulse with repetition 310 ms. Up to 4000 scans (20 minutes) were recorded. Approximate T_1 relaxation times for ^{15}N nucleus at T=303, 343, and 373 K were measured to be 53, 65, and 60 s., respectively. T_1 relaxation time of ^{14}N nucleus was measured at 383 K to be 21.0 ms. The coupling constant $^1J(^{15}N$-$^{14}N)$ was determined from line splitting in ^{15}N spectrum of the ^{14}N-^{15}N-^{15}N isotopomer at T=353 K to be 11.59 Hz.

3.3 Application of nuclear quadrupolar cross-correlations in the studies on the solution structure of bis(hexamethyldisilylamido)mercury(II).

In the present section, the approach similar to that used in the studies on **1** (see Section 3.1 and Ref. [28]), augmented with standard NMR relaxation measurements, will be applied to the problem of solution structure of bis(hexamethyldisilylamido)mercury(II) **3**. In neat liquids, the structure of **3** and its cadmium, and zinc analogs were once investigated using IR/Raman spectroscopy [44]. For all these compounds, it was concluded that the N-M-N chains are linear, and the $MNSi_2$ fragments are planar. Regarding the relative orientation of the $MNSi_2$ ligands, the IR/Raman mutual exclusion principle did not allow to discriminate between the eclipsed (D_{2h} symmetry) and staggered (D_{2d} symmetry) conformations (see Fig. 13). In gas phase, of the models with assumed D_{2h} and D_{2d} geometries of the Si_2NMNSi_2 skeleton only the latter could be satisfactorily brought into agreement with the experimental

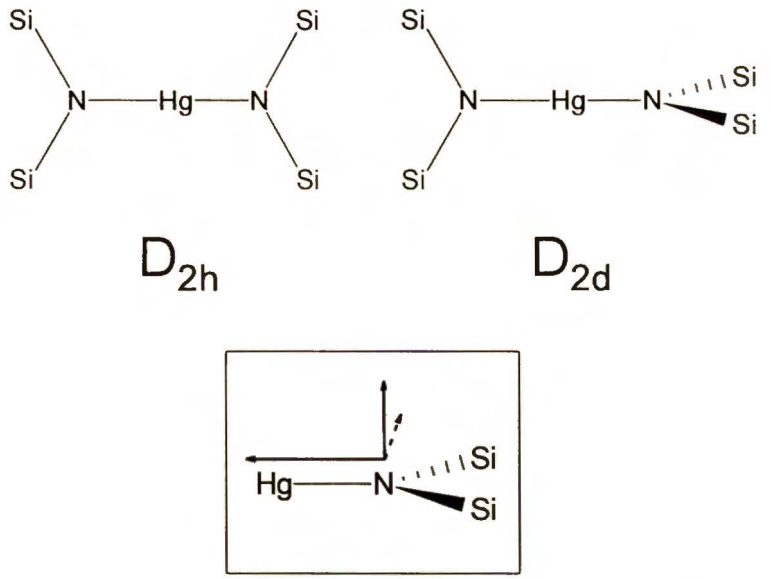

Figure 13: D_{2h} and D_{2d} conformations of **3**. Inset: Principal axes of the EFG tensors of the ^{14}N nuclei.

electron diffraction (ED) data for **3** [45] and its Zn [46] and Cd [47] analogs. However, in the final structure refinements it had proven advantageous to postulate the occurence of large amplitude librations around the N-M-N axis. The estimated librational energy barriers were low, about 8 ± 4 kJ mol^{-1}, and their origin was attributed to intramolecular steric rather than electronic effects [48]. In view of these findings, a straightforward extension of the above conclusions to the solution structures of the compounds in question did not seem justified. This was one of my motivations to undertake the present study on the solution structure of **3**.

3.3.1 Evaluation of quadrupolar cross-correlations.

In the molecule of **3**, the ^{199}Hg nucleus is the only candidate for the spy nucleus whose resonance lineshape is to provide information on the quadrupolar cross-correlation coefficient, r, for the pair of isochronous ^{14}N nuclei. Above room temperature, longitudinal relaxation times of the latter become long enough, compared with the magnitude of ^{1}J(^{199}Hg-^{14}N)=226 Hz calculated from the corresponding quantity in Table 3.6, for the lineshapes of ^{199}Hg to become increasingly informative, along with further temperature increase, about the magnitudes of r at the individual temperatures. The computer routine to iterative lineshape analysis, based on BWR theory, mentioned pre-

Table 3.6: Values of selected scalar nuclear spin-spin coupling constants in **3**.

Constant	Absolute value (Hz)
$^{1}J(^{199}Hg\text{-}^{15}N)^{a}$	316.2
$^{2}J(^{199}Hg\text{-}^{29}Si)^{b}$	32.8
$^{3}J(^{199}Hg\text{-}^{13}C)^{c}$	33.6
$^{1}J(^{29}Si\text{-}^{15}N)^{a}$	9.4
$^{1}J(^{29}Si\text{-}^{13}C)^{c}$	55.7
$^{2}J(^{15}N\text{-}^{14}N)^{d}$	< 9

[a] Measured directly from the ^{199}Hg and ^{29}Si satellites, respectively, in the natural abundance ^{15}N NMR spectrum (±0.2 Hz), recorded by the refocused INEPT pulse sequence (based on $^{3}J(^{15}N,Si,C,^{1}H) \simeq 1.8$ Hz) with ^{1}H decoupling.

[b] Measured directly from the ^{199}Hg satellites in the ^{29}Si NMR spectrum (±0.2 Hz), recorded by the refocused INEPT pulse sequence (based on $^{2}J(^{29}Si,C,^{1}H) = 7$ Hz), with ^{1}H decoupling.

[c] Measured directly from the ^{199}Hg and ^{29}Si satellites, respectively, in $^{13}C\{^{1}H\}$ NMR spectrum (±0.2 Hz).

[d] Determined from the spectrum at T=353 K using Eq. (38).

viously [27], is not applicable at hand to the present problem. This is because both ^{199}Hg and ^{14}N resonances in **3** are superpositions of contributions from a number of isotopomers in which these nuclei, beyond their mutual couplings, suffer additional scalar couplings to the ^{29}Si and ^{13}C nuclei. The relevant natural-abundance isotopomers of **3**, grouped into classes of the same spin coupling patterns to the ^{199}Hg and ^{14}N nuclei, are listed in Table 3.7. The above-mentioned computer routine was rendered capable of fitting a weighted sum of theoretical spectra, all of which are dependent on the same adjustable parameters, to the given experimental spectrum. Its capabilities were also extended to handle the spectra measured using the Hahn-echo technique. My earlier experience, gained from lineshape simulations described in Section 3.1.2, is that some lineshape details that are poorly marked in standard spectra usually undergo amplification when one uses such an experimental technique in which signal acquisition is delayed. In the present studies, due to accelerated quadrupolar relaxation, at temperatures below 333 K, the ^{199}Hg resonances gradually lack nontrivial features reflecting the degree of the qua-

Table 3.7: Natural-abundance isotopomers of **3** contributing to the observed ^{199}Hg and ^{14}N signals; spin-1/2 isotopes of Hg, Si and C are denoted by asterisks[a,b].

^{199}Hg signal	statistical weight (%)
$(C_3Si)_2NHg^*N(SiC_3)_2$	72.16
$(C_3Si)_2NHg^*N(Si^*C_3)(SiC_3)$	14.23
$(C_3Si)_2NHg^*N(SiC_2C^*)(SiC_3)$	9.70
$(C_3Si)_2NHg^*N(Si^*C_2C^*)(SiC_3)$ $(C_3Si)_2NHg^*N(SiC_2C*)(Si^*C_3)$ $(C_3Si)(C_3Si^*)NHg^*N(SiC_2C^*)(SiC_3)$	2.61
^{14}N signal	statistical weight (%)
$(C_3Si)_2NHgN(SiC_3)_2$	68.07
$(C_3Si)_2NHgN(Si^*C_3)(SiC_3)$	13.43
$(C_3Si)_2NHg^*N(SiC_3)_2$	12.82
$(C_3Si)_2NHg^*N(Si^*C_3)(SiC_3)$	2.4

[a] The ^{201}Hg isotope is treated as magnetically nonactive because of its large quadrupole moment and, accordingly, extremely rapid quadrupolar relaxation in compounds with non-spherical electric field symmetry at the nuclear site.

[b] Contributions from isotopomers whose relative abundances are below 1 per cent are neglected

drupolar cross-correlations while such features can still be discerned in the Hahn-echo spectra measured for appropriately long echo times. However, this gain in the information content is at the cost of a substantial enlongation of the experiment time, which is needed in order to achieve satisfactory signal-to-noise ratio. Therefore, under conditions where standard spectra contain enough information about r, there is no essential need to measure Hahn-echo spectra, unless the value of r is to be known with high accuracy.

In order to compare these two experimental approaches, at temperatures 383 and 403 K I measured both standard and Hahn-echo ^{199}Hg spectra. The latter were measured with τ delays of the lengths of 0.7 and 1.0 ms, respectively. The fitted values of r (the fits achieved are shown in Fig. 14) at 383 K are 0.761 ± 0.004, and 0.738 ± 0.007 for Hahn-echo and spectrum, respectively. At 403 K, the corresponding values are 0.740 ± 0.004 and 0.721 ± 0.006. However, it is remarkable that the estimates of r obtained from the Hahn-echo spectra come with the significantly smaller standard errors.

Actually, I was able to determine r with relatively high accuracy in the

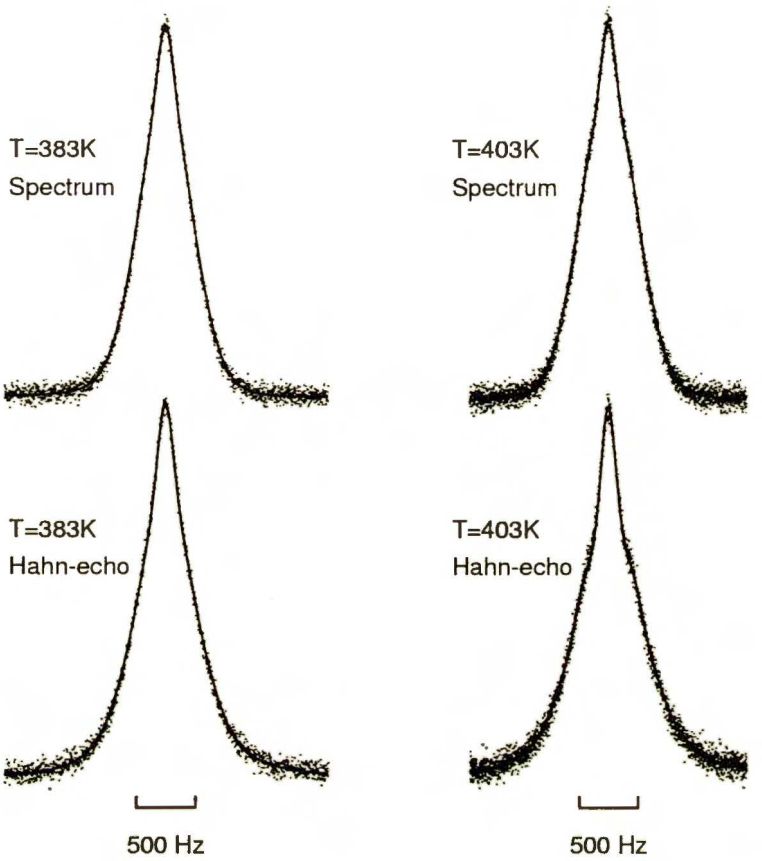

Figure 14: Standard and Hahn-echo spectra of **3** at temperatures 383 and 403 K. Delays τ were 0.7 and 1.0 ms, respectively. The theoretical "best fit" spectra are depicted by solid lines (see text for further comments).

range of 313 to 403 K, where the estimates of r at $T < 333$ K were obtained from Hahn-echo spectra. Results of the lineshape analyses are given in Table 3.8. My present way of proceeding was as follows: At each temperature, I first performed lineshape fits of the ^{14}N signal (the measurements of ^{199}Hz and ^{14}N spectra could be performed at exactly the same temperature because the same NMR probehead was used in each case). In these fits, the magnitudes of the relevant coupling constants were kept fixed; the only nontrivial parameter which was to be adjusted was the quadrupolar autocorrelation spectral density, j. From the theoretical considerations confirmed by numerical simulations it is known that in systems like that considered presently the signal of the quadrupolar nuclei is independent on the quadrupolar cross-correlation spectral density, k. The value of j was then used as a nonadjustable parame-

Table 3.8: Auto- and cross-correlation quadrupolar spectral densities obtained from lineshape fits of NMR spectra of ^{14}N and ^{199}Hg nuclei in **3**.

$T(K)$	$j(s^{-1})$	$k(s^{-1})$	r
313	169.46 ± 0.31	126.9 ± 1.3	0.749 ± 0.007
323	146.27 ± 0.25	111.8 ± 0.6	0.764 ± 0.004
333	128.55 ± 0.31	94.2 ± 0.6	0.733 ± 0.005
343	108.32 ± 0.25	84.2 ± 0.6	0.777 ± 0.006
363	85.07 ± 0.19	66.6 ± 0.6	0.783 ± 0.008
383[a]	67.92 ± 0.19	54.0 ± 0.6	0.795 ± 0.010
403[a]	54.73 ± 0.19	42.1 ± 0.6	0.769 ± 0.011

[a] The values obtained from standard spectra with considerably lower signal-to-noise ratios than those depicted in Fig. 14; note that these values are close to the corresponding values obtained from Hahn-echo spectra exhibiting a rather poor signal-to-noise ratio (see discussion on page 46)

ter in the lineshape fit of the ^{199}Hg signal. Here the only nontrivial adjustable parameter was k.

As was once deduced from the theoretical considerations [25], which were confirmed by my own theoretical (Section 3.1) and experimental findings described in Sections 3.2.1 and 3.2.2, the estimate of k delivered at convergence can be critically dependent on the absolute value of the J-coupling constant between the quadrupolar nuclei, especially in the instance where the latter are magnetically equivalent. In the present studies, I could only asses the absolute value of $J(^{14}N\text{-}^{14}N)$ to be smaller than 6 Hz (see Table 3.6). My estimates of k obtained assuming various values of $J(^{14}N\text{-}^{14}N)$ from the range 0-6 Hz did not differ among themselves by more than 0.5 per cent. However, assuming a unrealistic value of $J(^{14}N\text{-}^{14}N)$ to be greater than 30 Hz succeeds in an increase of the estimated value of k by more than 7 per cent. One more point that needs to be commented upon in the present context involves the impact on the estimated values of j and k of the line broadenings caused by factors other than quadrupolar relaxation. While the field inhomogeneity broadenings, the magnitudes of which I can asses to be smaller than 0.5 Hz, are of little significance, those originating from relatively fast ^{199}Hg relaxation, dominated by the CSA mechanism are non-negligible, especially at low temperatures. In order to make a proper account of these CSA-relaxation broadenings in

my lineshape fits, I performed independent measurements of the longitudinal relaxation times of ^{199}Hg, which are described below. In the lineshape fits, the CSA-relaxation effects on the ^{199}Hg resonances were accounted for as Lorentzian broadenings $w/2\pi(\mathrm{Hz}) = 7/(6\pi T_1)$ [2]. For selected temperatures, the experimental ^{199}Hg and ^{14}N spectra with the superimposed best fit theoretical spectra are displayed in Fig. 15.

It must be added that these solutions of the least-squares problems for the ^{199}Hg spetra are not unique. When negative values of k are assumed at the start, the corresponding values delivered at convergence are also negative, and their absolute magnitudes are nearly the same as those obtained from positive starting values. These negative solutions have been rejected since the corresponding rms errors were consistently larger, by 1 to 7 per cent, than those achieved for the respective positive solutions.

3.3.2 Longitudinal relaxation times.

T_1 relaxation times of ^{199}Hg in **3** were measured in temperature range of 243 to 403 K using the standard inversion recovery technique. In **3**, as in other covalent compounds of ^{199}Hg, the relaxation behavior of this nucleus is dominated by the CSA mechanism [49]. An Arrhenius plot of the observed ^{199}Hg relaxation rates is shown in Fig. 16. The deviations of the experimental relaxation rates from the least-squares straight line (described in the caption to Fig. 16) do not seem to bear a systematic character. They can be attributed to random errors in determining the integral intensities of the relatively broad ^{199}Hg resonances for the recovery times at which the magnetization recovery curves cross zero. At temperatures below the room temperature, the relaxation times of the ^{14}N nuclei become too short to be measured with reasonable accuracy using either the inversion recovery or the lineshape analysis technique. In this temperature range, the longitudinal relaxation times (and, in fact, the j parameters) were determined indirectly from lineshape fits of the ^{199}Hg signals. In these fits, the parameter j was varied while the values k were set equal to $\overline{r}j$, where $\overline{r}$ is an arithmetic average of the estimates of r obtained at temperatures above the room temperature. As in the lineshape fits carried out to determine r, the broadening of the ^{199}Hg spectra due to the CSA relaxation was calculated from the independently measured longitudinal relaxation times of the ^{199}Hg nucleus. The bias of the estimated values of j caused by fixing the magnitude of r is negligible since in the temperature range considered lineshapes of the ^{199}Hg spectra measured in the standard way are esentially insensitive to r. An Arrhenius plot of the longitudinal relaxation rates of the ^{14}N nuclei is shown in Fig. 16. As can be seen in Fig. 16, the experimental points are nearly perfectly aligned along a straight line. It is noteworthy that

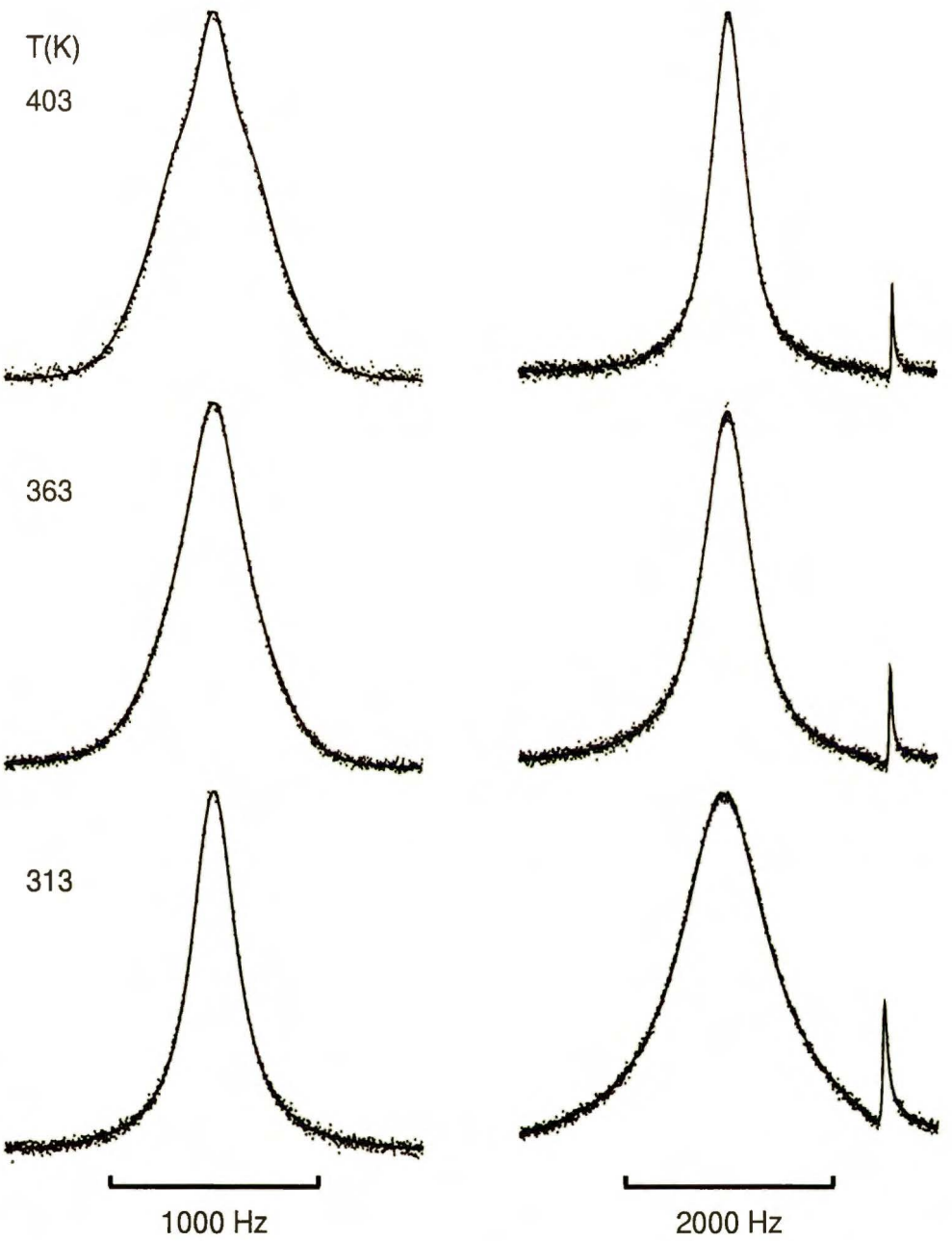

Figure 15: Experimental ^{199}Hg (left side) and ^{14}N (right side) spectra of toluene solution of **3** for selected temperatures, and the superimposed best fit theoretical spectra. The ^{199}Hg spectrum at T = 313 K is the Hahn echo spectrum (see text). Lorentzian lineshape was assumed for the narrow impurity signal (originating from admixture of the free ligand) in the ^{14}N spectra.

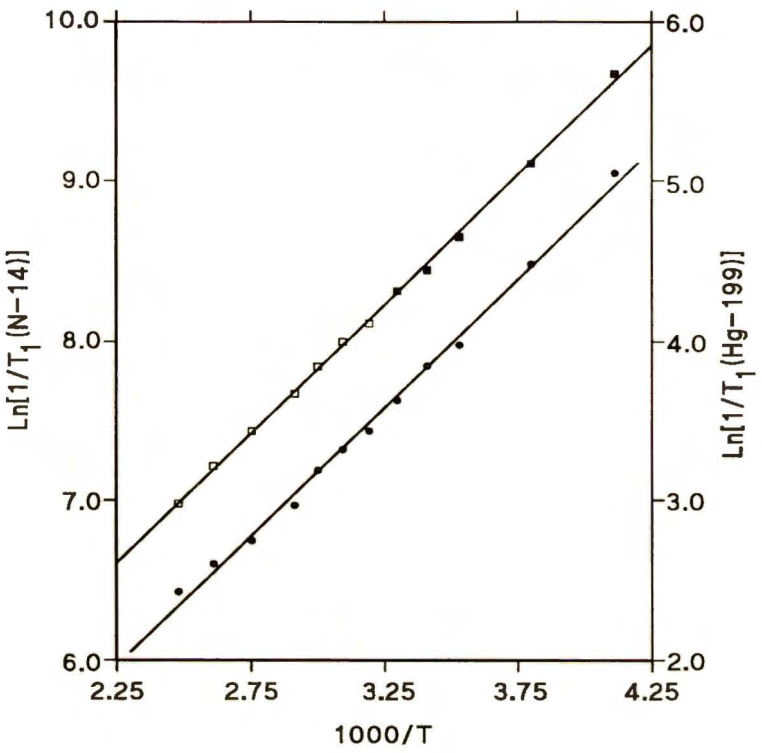

Figure 16: Arrhenius plots of the ^{199}Hg (solid circles) and ^{14}N (squares) relaxation rates $1/T_1$ (s^{-1}). The corresponding least-squares regression lines are : $\ln(T_1) = -(13.41 \pm 0.25 \text{ kJ mol}^{-1})/RT + (1.66 \pm 0.11)$ and $\ln(T_1) = -(13.49 \pm 0.13 \text{ kJ mol}^{-1})/RT - (2.96 \pm 0.06)$. Open and solid squares designate data obtained from lineshape fits of ^{14}N and ^{199}Hg spectra, respectively (see text).

the slope of the latter is practically identical with that of corresponding line for the ^{199}Hg relaxation rates (see caption to Fig. 16).

3.3.3 The ^{29}Si and ^{13}C spectra.

In both ^{29}Si and ^{13}C spectra, the satellite lines due to coupling with the ^{199}Hg nucleus do not show any extra broadening beyond that caused by relatively rapid longitudinal relaxation of ^{199}Hg. This holds true even for the highest temperature, T=403 K, at which such spectra were measured. These observations allow me to exclude the occurence of intermolecular ligand exchange; in the cadmium analog of **3**, such process does occur in toluene solutions of comparable molecular concentration, causing significant broadenings

and, at elevated temperatures, collapses of the corresponding ^{13}C and ^{29}Si doublets into singlets.

3.3.4 Discussion.

For a molecule whose structure is rigid on the timescale of molecular tumbling, cross-correlations between various time-dependent intramolecular interactions that contribute to nuclear spin relaxation are in general dependent on both geometrical and dynamic factors. These include orientations of the corresponding interaction tensors relative to the principal axis system of the rotational diffusion tensor, and the anisotropy of the latter. In the specific instance where such a molecule possesses symmetry center, the pairs of interactions whose respective tensors are transformed into each other under inversion in the center remain perfectly cross-correlated, regardless of what is the microscopic mechanism of rotational diffusion [11]. Such perfect cross-correlations will be maintained even in presence of intramolecular motions provided that the latter are sufficiently fast compared with the overall tumbling. In typical situations, upon changing the temperature the rates of the overall reorientation will be affected more substantially than those of the fast intramolecular processes. By an increase of temperature, the original disparity between the corresponding timescales may be diminished, which could manifest itself in a gradual decorrelation of the symmetry-related interactions. For the compound investigated presently, I was able to evaluate the quadrupolar cross-correlation coefficient, r, in the temperature range over which the overall tumbling, monitored by the ^{199}Hg relaxation rate (see below) is accellerated by more than a factor of 3. However, the estimated values of r, all of which fall below 0.8, do not show any systematic increase toward the limiting value 1 along with decreasing the temperature from 403 down to 313 K. Actually, to within the corresponding triple standard errors they remain independent of temperature. These observations can be rationalized if one assumes that the $Si_2NHgNSi_2$ skeleton behaves like a rigid body on the timescale of the molecular reorientations that are relevant for quadrupolar relaxation. In agreement with the inferences from the ED data for gas phase, the possibility that it exists in D_{2h} conformation ought to be excluded because the values of r are substantially different from 1. Moreover, regardless of what is the true conformation of **3**, the possibility that the EFG tensors for the ^{14}N nuclei are axially symmetric around the N-Hg-N axis should also be excluded since otherwise the values of r would be close to unity. However, the above conclusions are rather critically dependent on how realistic is the assumption about an essential rigidity of the $Si_2NHgNSi_2$ skeleton. In order to verify it further, I measured longitudinal relaxation times for the ^{14}N and ^{199}Hg nuclei, which

could be done over much broader temperature range, i.e. 243 to 403 K, than for r. Over the whole range, a perfect parallelism between the dependences on temperature of the ^{14}N and ^{199}Hg relaxation rates is maintained (see Fig. 16). As is pointed out below, this observation provides another essential argument against a flexibility of the $Si_2NHgNSi_2$ fragment (anticipated in view of the occurence of large-amplitude librations in gas phase) [45, 46, 47] on a timescale commensurable with that of molecular tumbling. Let me note that, due to the fact that the N-Hg bond is essentially a single bond [44, 48], the CSA tensor of the ^{199}Hg nucleus can to a good approximation be regarded as axially symmetric around the N-Hg-N axis, regardless of what is the true conformation of **3** (for D_{2d} conformation, this would be an exact symmetry). For any mutual orientation of the $HgNSi_2$ groups, the latter, which will further be referred to as Z axis, will remain an effective symmetry axis of the whole molecule. Hence, the relaxation behaviour of the ^{199}Hg nucleus will be controlled by reorientations around axes perpendicular to Z axis and will be insensitive to any motions around it. On the other hand, reorientations around Z must contribute to the relaxation rates of the ^{14}N nuclei, since the possibility for the EFG tensors to be axially symmetric with respect to the latter must be rejected (see above). Therefore, the parallelism between the ^{199}Hg and ^{14}N relaxation behaviours could be rationalized when reorientations around Z and around the axes perpendicular to it were controlled by the same microscopic mechanism. My experimental findings seem to confirm the occurence of such a single mechanism. Its temperature behaviour follows Arrhenius law rather closely, what can be seen from the Arrhenius plots of the ^{14}N and ^{199}Hg relaxation rates shown in Fig. 16, revealing the same activation energy of 13.4 kJ mol^{-1}. This points to an essential irrelevance for the observed relaxation effects of the possible large-amplitude librations around Z. In liquid phase, such librations can be considered in terms of some large-angle, rotational jumps modulating the small-angle, diffusional reorientations around Z. Such jumps would affect the ^{14}N relaxation rates only, via the asymmetries of the corresponding EFG tensors; because of axial symmetry around Z of the CSA tensor, they would not be reflected in relaxation rates of the ^{199}Hg nucleus. It is highly unlikely that the temperature dependence of such jumps be exactly the same as for diffusional reorientations. Thus, the temperature behaviour of the ^{14}N and ^{199}Hg relaxation rates discussed above, observed over temperature range exceeding 150 K, can be rationalized if the mean lifetime of the molecules of **3** between the possible large-angle jumps happens to be much longer than the orientational correlation time for the small-angle diffusion. This may mean that the relatively low, ca 8 kJ mol^{-1}, librational barrier found in gas phase [45] is substantially increased in liquid phase due to intermolecular in-

teractions. In conclusion, in the observed relaxation behaviour of the system discussed there are no such features that would necessitate going beyond the standard interpretation in terms of rotational diffusion. Moreover, the data collected reveal no flexibility of the $Si_2NHgNSi_2$ fragment on the timescale of the overall molecular tumbling. In view of what was pointed out at the beginning of this section, and of the fact that structures with the two NSi_2 groups permanently twisted relative to each other by angles different from 90 deg are highly improbable, one is left with the D_{2d} geometry as the only possibility for the conformation of the $Si_2NHgNSi_2$ skeleton. This is in agreement with the inferences from the gas phase studies [45, 46, 47]. Detailed questions regarding the nature of the reoriantational diffusion mechanism of the molecules of **3** and, more specifically, whether it is dominated by purely inertial[50, 39] or microviscosity effects[51, 52], must be left open. Nevertheles, in accord with D_{2d} geometry, axial symmetry around Z axis is to be assumed for the relevant rotational diffusion (RD) tensor; in what follows the two diffusion constants characterizing reorientations around Z, and around axes perpendicular to Z, will be denoted by $D_{\|}$ and $D_{\perp}$, respectively. Now, for each of the ^{14}N nuclei, one of the principal axes of its EFG tensor will be directed along Z while the two remaining axes, perpendicular to Z, will lie in the symmetry planes of the corresponding NSi_2 groups (see inset in Fig. 13). The system of the two principal axes perpendicular to Z of each EFG tensor is twisted by the angle of 90 deg relative to the corresponding system of the other. Using the expressions for auto- and cross-correlation spectral densities that are applicable to interaction tensors without axial symmetry (see Section 2.3) [15, 14], one can derive relationships connecting the observed values of r with both the RD anisotropy parameter $\xi = D_{\|}/D_{\perp}$ and the characteristics of the EFG tensors. For any such tensor, it is customary to label its principal axes in such a way that the absolute magnitudes of the corresponding principal values be ordered according Eq. (5) [5]. Then, the corresponding EFG asymmetry parameter η defined in Eq. (5) is nonnegative and never exceeds 1. Depending on which of the three principal EFG axes, x, y, and z, whose associated principal values obey Eq. (5), happens to coincide with the Z axis of the RD tensor, a different functonal dependence of r on η and ξ is obtained. All these three relationships can be described by a single expression

$$r = \frac{1 - \lambda_u(\eta)/(1+2\xi)}{1 + \lambda_u(\eta)/(1+2\xi)} \tag{39}$$

where for the orientations of $x \parallel Z$, $y \parallel Z$ and $z \parallel Z$, the corresponding functions λ_x, λ_y, and λ_z, are $[(3+\eta)/(1-\eta)]^2$, $[(3-\eta)/(1+\eta)]^2$ and η^2, respectively. My experimental results, combined with an assesment of the

probable magnitudes of the motional anisotropy parameter ξ, allow one to discriminate between these three orientations. Namely, if the gradient of the smallest magnitude was along Z axis (i.e., $x \parallel Z$), then only for the values of ξ exceeding 40 Eq. (39) would deliver physically sensible values of η (i.e., ones fulfilling $0 \leq \eta \leq 1$). It is worth noting that the smallest value of ξ, that is, ca. 40, would correspond to the limiting situation where each of the EFG tensors was axially symmetric ($\eta = 0$) around an axis perpendicular to Z (with the axes of the individual tensors subtending a dihedral angle of 90 deg, see above); for the values of η approaching 1 the corresponding values of ξ would tend to infinity. As is pointed out below, such an extent of rotational asymmetry for the molecules of **3** is extremely unlikely, so that the possibility of x being parallel to Z can be excluded. For the hypothetic orientation of $y \parallel Z$, the limiting values of ξ are about 4 (for $\eta = 1$) and about 40 (for $\eta = 0$, in which instance the orientations $y \parallel Z$ and $x \parallel Z$ become nondifferentiable by definition). It is illuminating to compare these estimates of ξ with the predictions derived from the two already invoked theoretical models of anisotropic rotational diffusion in liquids, the extended rotational diffusion (ERD) in the limit of small angle displacements[39], and hydrodynamic (HD)[51, 52] models. In the former, the anisotropy parameter ξ is given by the ratio of the corresponding principal values of the molecular inertia tensor I_X/I_Z ($= I_Y/I_Z$); for the gas-phase geometry of **3**, the value of ξ calculated in this way amounts to ca. 2.5. In various versions of the HD model, the motional anisotropy is related to the anisotropy of the molecular shape; for molecules of approximately spherical shape isotropic reorientation is predicted, regardless of the properties of the molecular inertia tensor. In the D_{2d} conformation, the molecules of **3** are approximately spherical. Moreover, they do not contain any peripheral functional groups that might engage in specific interactions with the solvent molecules, which would render the HD approach inapplicable. In any case, it seems reasonable to assume that the value of ξ falls somewhere between 1 (isotropic reorientation) and 2.5. Therefore, the possibility of $y \parallel Z$ can also be excluded and, accordingly, the most likely orientation of the EFG tensor for each of the ^{14}N nuclei is such that the axis of maximum gradient is directed along the N-Hg bond ($z \parallel Z$). Putting for r in Eq. (39) the arithmetic average of the corresponding values from Table 3.8., 0.77, the values of η falling in the range of 0.62 (for isotropic reorientation, $\xi = 1$) to 0.88 (for $\xi = 2.5$) are obtained. Thus, even such a non precise assessment of the reorientational asymmetry can yield reasonable estimates of η. To the best of my knowledge, this is the first attempt of determining the properties of an EFG tensor from quadrupolar cross-correlation effects in an isotropic liquid.

3.3.5 Concluding remarks.

The data on temperature dependences of both the quadrupolar cross-correlation and longitudinal relaxation of ^{14}N and ^{199}Hg nuclei for a toluene solution of **3** are shown to be consistent with the structure in which the Si_2N-Hg-NSi_2 skeleton maintains D_{2d} geometry on the time scale of overall molecular reorientation. The extent of the possible anisotropy of the latter, described by the ratio $\xi = D_{||}/D_{\perp}$ of the relevant rotational diffusion constants, must be confined to relatively narrow limits: from isotropic reorientation ($\xi = 1$) expected from hydrodynamic models to the anisotropy controlled by the properties of the moment of inertia tensor, in which case ξ ought not to exceed 2.5. Accordingly, the principal axes of the ^{14}N EFG tensors, concerned with gradients of maximum absolute values, can uniquely be located along the direction of the N-Hg-N chain. The value of the EFG asymmetry parameter, calculated from the experimental data assuming isotropic reorientation, amounts to 0.62. The present work seems to provide the first evidence of the utility of quadrupolar cross-correlaion effects for structural studies in isotropic liquids.

3.3.6 Experimental.

The compound **3**, which is a non-volatile liquid under ambient conditions (m.p. 12°C), was synthesized and purified according to a published procedure [44]. All of the NMR data referred to in the present work were obtained for a 1 mol/liter solution of **3** in toluene-d8, sealed in NMR tube (o.d. 5 mm) under argon at ambient pressure. NMR measurements were performed on a Bruker DRX 250 and Bruker DRX 500 MHz spectrometers. All variable temperature measurements were performed on the latter machine equipped with temperature control unit BVT 3000. The sample temperature was determined from reads of a thermocouple placed within the NMR probehead which were calibrated against the methanol (for $T < 303$ K) and ethylene glycol ($T > 303$ K) chemical shift thermometers. The ^{199}Hg and ^{14}N spectra to be subject to iterative lineshape analysis were obtained by collecting data from 100000-400000 and 4000-10000 scans, respectively. The spectra of ^{15}N at natural abundance, measured to determine scalar couplings (J-couplings) to the nitrogen atoms, were obtained by collecting 10000 scans. Values of the scalar coupling constants that are relevant for the lineshape analysis are listed in Table 3.6.

4 Conclusions.

The investigations performed by me state a basis to draw the following general conclusions:

- Scalar coupling between magnetically equivalent nuclei can in certain conditions significantly influence the NMR spectra.
- Cross-correlation spectral densities of quadrupolar interactions can be determined in the investigated type of systems, with good accuracy, from spectra of an appropriate "spy nucleus".
- Nuclear quadrupolar cross-correlations can be a very useful tool in studies on molecular structure and dynamics in isotropic solvents.
- In cases where standard spectra do not carry enough information about the investigated quantities such as the coefficient r, the Hahn-echo pulse sequence can be applied in order to amplify the impact of these quantities on the observed signal.

Of the detailed results obtained in this thesis, it is worth to emphasize the following:

- The azide anion ^{14}N-^{15}N-^{14}N retains a $D_{\infty h}$ symmetry not only on the NMR time scale, but also on the time scale of molecular tumbling.
- In toluene solution, on the time scale of molecular tumbling, the molecule of bis(hexamethyldisilylamido)mercury(II) has a D_{2d} symmetry rather than that D_{2h}.
- The determined asymmetry, η, of the EFG tensor of the nitrogen atom in bis(hexamethyldisilylamido)mercury(II) is found to fall between 0.62 and 0.88; the direction of the z axis of this tensor lies along the N-Hg bond.
- A very good agreement was found between both the measured and theoretically calculated values of the quadrupolar cross-correlation coefficient, r, for the pair of magnetically equivalent ^{14}N nuclei in 2,1,3-benzoselenadiazole dissolved in toluene and benzene.

References

[1] S. A. Smith, W. E. Palke and J. T. Gerig, *Concepts Magn. Reson.* **4,** 107 (1992).

[2] A. Abragam, "The Principles of Nuclear Magnetism," Oxford Univ. Press, Oxford, 1961, Chap. 8.

[3] J. M. Lehn and J. P. Kintzinger, in "Nitrogen NMR," (ed. M. Witanowski and G. A. Webb), Plenum Press, London, 1973, Chap. 3.

[4] C. P. Slichter, "Principles of Magnetic Resonance," Springer-Verlag, Berlin, 1978, Chap. 9.

[5] A. Abragam, "The Principles of Nuclear Magnetism," Oxford Univ. Press, Oxford, 1961, Chap. 7.

[6] R. K. Wangsness and F. Bloch, *Phys. Rev.* **89,** 728 (1953); F. Bloch, *Phys. Rev.* **102,** 204 (1956); *Phys. Rev.* **105,** 1206 (1957).

[7] A. G. Redfield, *Adv. Magn. Reson.* **1,** 1 (1965).

[8] K. Blum, "Density Matrix. Theory and Applications," Plenum Press, New York, 1981, Chap. 2.

[9] U. Fano, "Lectures on the Many-Body Problem," (ed. E. R. Caianiello), Vol. 2, Academic Press, New York, 1964, p. 217.

[10] J. Jeener, *Adv. Magn. Reson.* **10,** 2 (1982).

[11] S. Szymański, A. M. Gryff-Keller, and G. Binsch, *J. Magn. Reson.* **68,** 399 (1986).

[12] P. S. Hubbard, *Phys. Rev.* **180,** 319 (1969).

[13] H. W. Spiess, in "NMR. Basic Principles and Progress", Vol. 15 (ed. P. Diehl, E. Fluck, and R. Kosfeld), Springer-Verlag, Berlin, 1978, Chap. 4.

[14] L. G. Werbelow, in "Nuclear Magnetic Resonance Probes of Molecular Dynamics" (ed. R. Tycko), Kluwer Academic, Dordrecht, 1994, Chap. 5.

[15] D. Canet, *Concepts Magn. Reson.* **10,** 291 (1998).

[16] W. T. Huntress, "Advances in Magnetic Resonance" Vol. 4, Academic Press, New York, 1970, p. 1.

[17] L. D. Favro, *Phys. Rev.* **119,** 53 (1960).

[18] D. E. Woessner, *J. Chem. Phys.* **37,** 647 (1962).

[19] W. T. Huntress, *J. Chem. Phys.* **48,** 3524 (1968).

[20] P. S. Hubbard, *J. Chem. Phys.* **52,** 563 (1970).

[21] R. L. Vold, R. R. Vold, R. Poupko, and G. Bodenhausen, *J. Magn. Reson.* **38,** 141 (1980).

[22] R. Poupko, R. L. Vold, and R. R. Vold *J. Magn. Reson.* **34,** 67 (1979).

[23] D. Jaffe, R. L. Vold, and R. R. Vold *J. Chem. Phys.* **78,** 4852 (1983).

[24] L. G. Werbelow, G. A. Morris, P. Kumar, and J. Kowalewski, *J. Magn. Reson.* **140,** 1 (1999).

[25] S. Szymański, *J. Magn. Reson.* **127,** 199 (1997).

[26] A. Kumar, R. Christy Rani Grace, and P. K. Madhu, *Prog. NMR Spectrosc.* **37,** 191 (2000).

[27] S. Szymański, FORTRAN routines to simulations and iterative analysis of NMR spectra (unpublished).

[28] P. Bernatowicz, O. Bjørlo, E. H. Mørkved, and S. Szymański, *J. Magn. Reson.* **145,** 152 (2000).

[29] P. Bernatowicz and S. Szymański, *J. Magn. Reson.* **148,** 455 (2001).

[30] L. G. Werbelow, in "Encyclopedia of Nuclear Magnetic Resonance", (ed. D. M. Grant and R. K. Harris), Wiley, Chichester, 1980, p. 4092.

[31] S. Szymański and A. M. Gryff-Keller, *J. Magn. Reson.* **16,** 182 (1974).

[32] H. Günther, "NMR Spectroscopy: An Introduction," Wiley, Chichester, 1980, Chap. 4.

[33] R. R. Ernst, G. Bodenhausen, and A. Wokaun, "Principles of Nuclear Magnetic Resonance in One and Two dimensions", Clarendon Press, Oxford, 1987, p. 208.

[34] H. Duddeck, *Prog. NMR Spectrosc.* **27,** 1 (1995).

[35] E. H. Mørkved, O. Bjørlo, W. Schilf, and P. Bernatowicz, *Bull. Pol. Acad. Sci. (Chem.)* **48,** 47 (2000).

[36] V. G. Malkin, O. L. Malkina, M. E. Casida, and D. R. Salahub, *J. Am. Chem. Soc.* **116,** 5898 (1994).

[37] R. Ahlrichs, M. Bär, M. Höser, and C. Kölmel *Chem. Phys. Lett.* **162,** 165 (1989).

[38] A. D. Bain and G. J. Duns, *J. Magn. Reson. A* **112,** 258 (1995).

[39] R. E. D. McClung, *Advan. Mol. Relaxation Interaction Processes* **10,** 83 (1977).

[40] O. Hinsberg, *Ber. Dtsch. Chem. Ges.* **22,** 862 (1889); *Ber. Dtsch. Chem. Ges.* **22,** 2895 (1889).

[41] M. Witanowski, L. Stefaniak, S. Szymański, and H. Januszewski, *J. Magn. Reson.* **28,** 217 (1977).

[42] J. Muller and H. F. Schroder, *Z. Anorg. Allg. Chem.* **450,** 149 (1979).

[43] K. Clusius and M. Vecchi, *Ann. Chem.* **607,** 17 (1957).

[44] H. Burger, W. Sawodny, and U. Wannagat, *J. Organomet. Chem.* **3,** 113 (1965).

[45] E. C. Alyea, K. J. Fisher, and T. Fjeldberg, *J. Mol. Struct.* **130,** 263 (1985).

[46] A. Haaland, K. Hedberg, and P. P. Power, *Inorg. Chem.* **23,** 1972 (1984).

[47] E. C. Alyea, K. J. Fisher, and T. Fjeldberg, *J. Mol. Struct.* **127,** 325 (1985).

[48] D. H. Harris, M. F. Lappert, J. B. Pedley, and G. J. Sharp, *J. Chem. Soc. , Dalton Trans.* 945 (1976).

[49] R. Benn, H. Günther, A. Märcker, V. Menger, and P. Schmitt, *Angew. Chem.* **94,** 314 (1982); *Angew. Chem. Int. Ed. Engl.* **21,** 295 (1982).

[50] R. G. Gordon, *J. Chem. Phys.* **44,** 1830 (1966).

[51] G. K. Youngren, A. J. Acrivos, *Chem. Phys.* **63,** 3846 (1975).

[52] R. P. Klüner, A. J. Dölle, *J. Phys. Chem. A* **101,** 1657 (1997).